

Topical Hidden Genome: Discovering Latent Cancer Mutational Topics using a Bayesian Multilevel Context-learning Approach

Saptarshi Chakraborty* Zoe Guan[†] Colin B. Begg[‡] Ronglai Shen[§]

Abstract

Statistical inference on the cancer-site specificities of collective ultra-rare whole genome somatic mutations is an open problem. Traditional statistical methods cannot handle whole-genome mutation data due to their ultra-high-dimensionality and extreme data sparsity – e.g., >30 million unique variants are observed in the ~1700 whole-genome tumor dataset considered herein, of which >99% variants are encountered only once. To harness information in these rare variants we have recently proposed the “hidden genome model”, a formal multilevel multi-logistic model that mines information in ultra-rare somatic variants to characterize tumor types. The model condenses signals in rare variants through a hierarchical layer leveraging contexts of individual mutations. The model is currently implemented using consistent, scalable point estimation techniques that can handle 10s of millions of variants detected across thousands of tumors. Our recent publications have evidenced its impressive accuracy and attributability at scale. However, principled statistical inference from the model is infeasible due to the volume, correlation, and non-interpretability of the mutation contexts. In this paper we propose a novel framework that leverages topic models from the field of computational linguistics to induce an *interpretable dimension reduction* of the mutation contexts used in the model. The proposed model is implemented using an efficient MCMC algorithm that permits rigorous full Bayesian inference at a scale that is orders of magnitude beyond the capability of out-of-the-box high-dimensional multi-class regression methods and software. We employ our model on the Pan Cancer Analysis of Whole Genomes (PCAWG) dataset, and our results reveal interesting novel insights.

1 Introduction

A large and growing body of research has documented strong links between specific somatic mutations and cancer types (Haigis, Cichowski, and Elledge 2019). This has put forward an emerging field aiming to characterize cancer types through tumor mutation footprints. Some notable clinical applications are as follows: (a) predicting primary sites of origin of metastasized tumors of uncertain

*Department of Biostatistics, State University of New York at Buffalo, chakrab2@buffalo.edu

[†]Department of Epidemiology & Biostatistics, Memorial Sloan-Kettering Cancer Center, guanz@mskcc.org

[‡]Department of Epidemiology & Biostatistics, Memorial Sloan-Kettering Cancer Center, beggc@mskcc.org

[§]Department of Epidemiology & Biostatistics, Memorial Sloan-Kettering Cancer Center, shenr@mskcc.org

primaries, a major clinical task involving 3-5% of all cancer diagnoses worldwide; (b) accurate prognostication of rare, phenotypically heterogeneous cancer, and (c) early detection of cancer from liquid biopsies through circulating tumor DNAs (ctDNAs) in the bloodstream. The mutation driven cancer-site characterization framework may provide rigorous statistical answers to these pertinent questions.

The existing research in this area has two broad ends. On the *clinical* end lie studies considering prediction of tumors based on their mutation footprints (Soh et al. 2017; Jiao et al. 2020). These studies train classification models, typically blackbox methods such as deep learning, support vector machine, random forest etc., on somatic mutation data and then use the trained models to predict cancer types of new tumors. These “pure prediction algorithms” permit high predictive accuracy in specific examples, but they lack interpretation, attribution (Efron 2020) and inference, and may produce results that are unreliable for clinical tasks (Lapusckin et al. 2019).

By contrast, on the *scientific end* lie studies investigating and quantifying associations between specific mutations and cancer to derive a curated list of specific genomic regions, e.g., of cancer genes (Chakravarty et al. 2017), and subsequently utilizing this curated list to understand the biology of cancer risk (Soh et al. 2017; Haigis, Cichowski, and Elledge 2019). These studies typically focus on a handful of recurring variants/genomic regions to infer their tissue site-specificities via some established inferential methods, but ignore the rare and previously unobserved variants. This, in part, is due to the lack of statistical methods available for handling ultra-high dimensional and rare somatic mutations. Indeed, the vast majority of whole genome alterations are ultra-sparse – e.g., <1% of the >35 million of variants cataloged in the PCAWG data (Campbell et al. 2020) considered herein comprising >1500 tumors were detected in more than one tumor. Novel mutations are also routinely discovered in new sequencing studies. Such data are not suited for traditional inferential statistical methods. However, when harnessed via appropriate signal condensation tools such as the *Good-Turing* empirical Bayes probability estimates, strong tissue-specific information can be extracted from rare variants, as demonstrated in our earlier empirical study (Chakraborty et al. 2019).

Within this framework, we have recently proposed the *hidden genome model* (Chakraborty, Begg, and Shen 2020), a formal multilevel multinomial logistic model that characterizes cancer types by using the tumor’s entire somatic mutation fingerprint including the ultra-sparse variants as predictors. To harness this ultra-massive predictor space the model employs *context-based feature condensation*. More precisely, it employs in a hierarchical layer *meta-features* describing individual variants – such as gene labels, types of single base substitution (SBS; 96 possible types), topological positions on the chromosome, and various epigenetic features – to model the regression effects of the individual variants themselves (see Section 3.3). This contextualization is based on an intuitive observation: for the vast majority of individual variants, including all rare variants, mutation contexts can describe collectively the entirety of their tissue-specific effects, with only a handful of frequent variants exhibiting strong residual effects that are not explained by their contexts

alone. This contextualization aids highly informative predictor dimension reduction – condensing information in 10s of millions of individual variants into a few thousand meta-features. This, together with appropriately defined sparsity inducing layers in the model effectuates stable, consistent, and highly scalable (marginal maximum a posteriori) point estimation using group-lasso (Yuan and Lin 2006) regularized multi-logit likelihood maximization. The model has been successfully employed on whole genome data with >20 million variants (Chakraborty, Martin, et al. 2021), and also in targeted gene-panel based clinical cancer research setting (Chakraborty, Ecker, et al. 2021) and has provided rigorous quantification of tissue-specificities of collective mutations while permitting impressive prediction/classification accuracy in each application.

However, quantifying estimation uncertainty for statistically stable and biologically meaningful inference is currently infeasible for two primary reasons. First, the parameters associated with the meta-feature categories, while aiding substantial dimension reduction for point estimation, are still too voluminous (in the order of $K \times 1000$ s, K being the number of cancer categories) for MCMC-based full Bayesian implementation of the multi-level model. Second, the correlatedness and lack of biological interpretability of individual mutation context categories such as the *observed* 96 SBS types and the windowed positions on the chromosomes, preclude scientifically meaningful inference.

In this paper, we posit a novel methodological framework that builds upon this previous work, introducing new key structures that collectively permit *interpretable* and *practicable* (full) Bayesian inference at scale. The framework proposes *interpretable dimension reduction* of meta-feature categories leveraging topic models from computational linguistics (Blei and Lafferty 2009). Analogous to word topics in computational linguistics, which are latent lower dimensional embeddings that group “similar” individual words with common underlying semantics, meta-feature topics are embeddings of “similar” meta-feature categories (e.g., specific genes or specific chromosome windows); where the “similarity” is measured with a view to tumor type specificities of associated mutations. The meta-feature topics share important analogies with *mutation signatures* in genomics, latent structures derived from the observed SBS-96 categories. We note however that herein we employ a generalized notion of topics that applies beyond SBS as typically considered in genomics; our framework caters to any categorical meta-feature source such as genes and chromosome regions.

In our experience to date the prominent meta-feature topics are substantially lower dimensional (typically <300 in number) and much less correlated than the original meta-feature categories. This effectuates impressive bi-level dimension-reduction in the classification model: first from the variants (10s of millions) to the observed meta-features (a few thousands) and then from the observed meta-features to the latent meta-feature topics (typically <300). The regression coefficients of the original “observed” meta-features can then be derived as linear combinations of the reduced meta-feature regression coefficients (c.f. principal component regression) to quantify observed meta-feature effects, and to also readily permit full Bayesian posterior prediction from the model on new datasets. For the substantially reduced-dimensional “independent” predictor effects (i.e.,

latent topic effects and *residual variant effects*, see Section 3.2) a Bayesian group-lasso prior can be elicited for stable estimation and prediction. Note that both the topic modeling of observed meta-feature categories, and subsequent hidden genome modeling with meta-feature topics are done in a single, fully connected multilevel model that permits coherent, rigorous full Bayesian inference. For implementation, we propose an efficient Metropolis-within-Gibbs sampler leveraging bi-level data augmentation Kyung et al. (2010). This permits theoretical guarantees associated with MCMC methods for accurate posterior inference.

For expository purposes we employ our method on 1706 tumors from 10 separate cancer sites sequenced in the Pan Cancer Analysis of Whole Genomes (PCAWG) study, collectively utilizing >35 million unique variants as predictors (see Section 2 for a detailed note on the dataset). Our results reveal interesting novel insights. To assess interpretability/reproducibility of our results we validate our findings through multi-fold followup analyses. For the whole genome chromosome window topics, in the absence of a direct validation dataset, we validate our findings through association with certain epigenetic features. For exome level SBS topics, we perform two direct independent validations using (a) the publicly deposited COSMIC mutation signatures, and (b) estimated SBS topics obtained from our model employed on the Cancer Genome Atlas (TCGA) dataset (subsetting to the same 10 cancer sites as in the training PCAWG data).

2 Data Description and Problem Overview

Our primary motivating dataset is from Pan Cancer Analysis of Whole Genomes (PCAWG) (Campbell et al. 2020). For expository purposes here we focus on 10 common cancer sites cataloged in the dataset with at least a moderate sample size (n) each: liver ($n=349$), pancreatic ($n=326$), prostate ($n=286$), breast ($n=214$), ovarian ($n=113$), kidney ($n=111$), skin ($n=107$), esophageal ($n=98$), colorectal ($n=60$), and lung ($n=38$). A total of 36,325,180 variants, with 35,285,233 observed only once, were detected by a consensus mutation calling approach on these 1,702 tumors: an average of 19,076 variants per tumor. To understand variant tissue specificities based on smaller genotyping panels, we consider two subsetting versions of the whole genome data – a version to simulate a whole exome panel (Bailey et al. 2018), and a version to simulate a targeted cancer gene panel (Zehir et al. 2017). Our objective is to perform multinomial regression characterizing the cancer type of a tumor as a function of its mutation footprint (cataloged by the three panels) while permitting rigorous statistical inference. However, the key challenge is of course the ultra high-dimensionality and extreme predictor sparsity. As noted, we propose to solve this problem by introducing hierarchical layers in the regression model aiding detection and utilization of latent, lower dimensional meta-feature *topics*.

3 Full Bayesian Inference on Tissue-Specificities of Whole Genome Mutations

3.1 Notation and Setup

Consider a training dataset comprising N tumors indexed $n = 1, \dots, N$ with $c_n \in \{1, \dots, K\}$ denoting the known cancer site/class label for tumor n , where K is the total number of cancer sites. Label the J distinct mutations observed in the training dataset as $j = 1, \dots, J$; let x_{nj} be a binary indicator of the presence of the j -th mutation in the n -th tumor ($1 \equiv$ presence; $0 \equiv$ absence) and let $M_n = \sum_{j=1}^J x_{nj}$ be the total mutation burden in tumor n . Construct the $N \times J$ variant design matrix X by stacking $x_n = (x_{n1}, \dots, x_{nJ})^T$ as rows: $X = ((x_{nj}))$. Thus, $e_{n;N}^T X = x_n^T$ where $e_{n;N}$ denotes the N -component unit vector whose n -th component is 1 and the remaining components are 0. We are interested in regressing the cancer site labels $\{c_n\}$ on the mutation occurrences $\{x_{nj}\}$, to (a) jointly infer the tissue-site specificities of the individual mutations $\{j\}$, and (b) predict the cancer label $c_{n'}$ of a new (test set) tumor $n' \notin \{1, \dots, N\}$ through its mutational footprint $x_{n'}$. Note that the new tumor n' may feature hitherto unobserved mutations $\{j'\} \notin \{1, \dots, J\}$, and our regression model needs to appropriately acknowledge this possibility. Below we review the hidden genome model (Chakraborty, Begg, and Shen 2020) that utilizes contextualization of variants for this purpose.

3.2 Contextualization via meta-features

The hidden genome model leverages *meta-features*, higher level features about the individual variants themselves, embodying mutation contexts. These meta-features are available for all variants, including rare variants observed in the training data and new variants appearing only in the prediction (test) data. Genomic meta-features are commonly categorical, but they may also be continuous. Examples of categorical meta-features include the gene itself, single base substitution types (SBS; 96 possible types), and topological position on the chromosome (e.g., location among ~ 3000 1-megabase length windows). Examples of continuous meta-features include epigenomic feature scores such as histone marks and chromatin accessibility. Here we focus primarily on categorical meta-features to aid topic model based dimension reduction. Continuous meta-feature variables, if present, can be directly incorporated without topic modeling into the hidden genome framework following Chakraborty, Martin, et al. (2021).

To aid distinction we use the term *meta-feature source* to denote a specific meta-feature variable (e.g., gene, chromosome window) and *meta-feature categories* to denote individual categories of a meta-feature source (e.g., gene *KRAS*, chromosome 1 window 1 etc.). Individual meta-feature categories from *all* meta-feature sources are combined to produce say P total categories labeled as $1, 2, \dots, P$. Subsequently we create dummy coded (“one-hot” encoded) binary indicators cataloging correspondence between individual variants and meta-feature categories. For variant j let $u_j = (u_{j1}, \dots, u_{jP})$ be meta-feature indicators with u_{jp} being 1 if the j -th variant is associated with

meta-feature category p and 0 otherwise. Continuous meta-feature values for variant j , if present, are subsequently appended to u_j . Finally we construct the meta-design matrix U by stacking u_j as rows: $U = ((u_{jp}))$. The key idea behind the hidden genome model is to quantify the tissue-specific effects of individual variants via a meta-feature regression based on the meta-feature design matrix U .

3.3 A brief review of the point-estimated hidden genome cancer site classification model

We briefly review below the multilevel *hidden genome model* and its point estimation as suggested in Chakraborty, Begg, and Shen (2020). The likelihood layer of the model considers a multi-logistic regression connecting the cancer type probability $\Pr(c_n = k)$ to the observed variant indicators $\{x_{nj}\}$. A subsequent hierarchical *meta-feature regression* layer connects variant j and cancer site k -specific regression coefficient β_{jk} to variant j specific meta-features u_j as $\beta_{jk} = u_j^T \omega_{\bullet,k} + \beta_{j,k}^0$ where $\omega_{\bullet,k} = (\omega_{p,k})_{p=1,\dots,P}$ is the vector of meta-feature effects specific to cancer site k , and $\beta_{j,k}^0$ is the *residual effect* of variant j in cancer site k that is *not* explained by the context. Finally, a group lasso prior for $\{\beta_{j,k}^0\}$ and $\{\omega_{p,k}\}$ is considered for regularized estimation. The model is succinctly expressed as follows.

$$\Pr(c_n = k) = \frac{\exp[\alpha_k + e_{n;N}^T X \beta_{\bullet,k}]}{\exp[\sum_{k'=1}^K \alpha_{k'} + e_{n;N}^T X \beta_{\bullet,k'}]} \quad (3.3.1)$$

$$\beta_{j,k} = u_j^T \omega_{\bullet,k} + \beta_{j,k}^0 \quad (3.3.2)$$

$$\beta_{jk}^0 \sim \text{N}(0, \tau_{j;\beta^0}^2); \omega_{pk} \sim \text{N}(0, \tau_{p;\omega}^2); \tau_{j;\omega}^2, \tau_{p;\theta}^2 \sim \text{Gamma}((K+1)/2, \lambda^2). \quad (3.3.3)$$

The key meta-feature-regression layer (3.3.2) regresses $\{\beta_{jk}\}$ on the contexts $\{u_j\}$ effectuating signal condensation in all, including rare, variants. The residual effects $\{\beta_{jk}^0\}$ are non-zero and indeed can be realistically be estimated for only a few strongly discriminative non-rare variants. Following computation of the XU matrix arising after substituting (3.3.2) into (3.3.1), one may therefore perform a feature screening to keep all but a few recurring tissue-specific variants for estimation of their $\beta_{j,k}^0$. For scalable point estimation of the model Chakraborty, Begg, and Shen (2020) marginalize out all but the key parameters of interest, viz., α, β^0, ω , given the sparsity level

parameter λ to produce the following log marginal posterior density.

$$\begin{aligned} & \log \pi(\alpha, \beta^0, \omega \mid \lambda, c_1, \dots, c_n, x_1, \dots, x_n) \\ &= \sum_{n=1}^N \sum_{k=1}^K 1(c_n = k) \log \left(\frac{\exp \left[\alpha_k + e_{n;N}^T X U \omega_{\bullet,k} + e_{n;N}^T X \beta_{j,k}^0 \right]}{\exp \left[\sum_{k'=1}^K \alpha_{k'} + e_{n;N}^T X U \omega_{\bullet,k'} + e_{n;N}^T X \beta_{j,k'}^0 \right]} \right) \\ & \quad - \lambda \sum_{j=1}^J \|\beta_{j,\bullet}^0\|_2 - \lambda \sum_{p=1}^P \|\omega_{p,\bullet}\|_2. \end{aligned}$$

This is a group lasso penalized multi-logistic log-likelihood with intercept α , and regression coefficients β and ω with associated predictors x_n and $x_n^T U$ respectively, and penalty parameter λ . The corresponding (marginal) posterior mode can be efficiently computed using existing software (Friedman, Hastie, and Tibshirani 2010), and consistency of the resulting estimates follow from group-lasso theory. Note however that uncertainty quantification for statistical inference in this framework is infeasible due to voluminousness of the meta-feature categories.

3.4 The topical hidden genome: a Bayesian multilevel model with interpretable contexts

At the outset, we deviate from Chakraborty, Begg, and Shen (2020) by using instead a normalized version of the predictor $\{\tilde{x}_{nj} = x_{nj}/M_n\}$ measuring proportions of total mutation burden M_n attributable to individual variants $\{j\}$ and producing a normalized version \tilde{X} of the variant design matrix. This normalization acknowledges mutation burden heterogeneity observed in large-scale genomic data. Furthermore, it aids a product matrix $\tilde{X}U$ whose columns catalog analogous proportions of $\{M_n\}$ attributable to individual meta-feature categories. Next, we embed into the hidden genome model a hierarchical topic model layer for interpretable dimension reduction of the mutation context categories. For notational simplicity below we restrict to a *single, categorical meta-feature source* (e.g., only SBS) for the model; a generalization with several categorical and continuous meta-feature sources is described in Section 3.6. The proposed *topical hidden genome model* is first succinctly expressed as follows.

$$\Pr(c_n = k) = \frac{\exp \left[\alpha_k + e_{n;N}^T \tilde{X} \beta_{\bullet,k} \right]}{\exp \left[\sum_{k'=1}^K \alpha_{k'} + e_{n;N}^T \tilde{X} \beta_{\bullet,k'} \right]} \quad (3.4.1)$$

$$\beta_{j,k} = \beta_{j,k}^0 + u_j^T \omega_{\bullet,k} \quad (3.4.2)$$

$$\omega_{\bullet,k} = W^{-1} \theta_{\bullet,k} \quad \left(\implies W \omega_{\bullet,k} = \theta_{\bullet,k}; W^{-1} = W^T (W W^T)^{-1} \right) \quad (3.4.3)$$

$$\alpha_k \sim \text{N}(0, \tau_{0;\alpha}^2) \quad (3.4.4)$$

$$\beta_{jk}^0 \sim \text{N} \left(0, \frac{\tau_{j;\beta^0}^2}{\tilde{\sigma}_{\text{obs},j}^2} \right); \theta_{sk} \sim \text{N} \left(0, \frac{\tau_{s;\theta}^2}{\tilde{\sigma}_{\text{topic},s}^2} \right); \tau_{j;\beta^0}^2, \tau_{s;\theta}^2 \sim \text{Gamma} \left(\frac{K+1}{2}, \frac{\lambda^2}{2} \right) \quad (3.4.5)$$

$$\text{with } \tilde{\sigma}_{\text{obs},j} = \hat{\text{sd}}(\tilde{X}_{\bullet,j}); \tilde{\sigma}_{\text{topic},s} = \hat{\text{sd}}\left(\left[\tilde{X}UW^{-}\right]_{\bullet,s}\right)$$

$$\lambda^2 \sim \text{Gamma}(a_\lambda, b_\lambda) \tag{3.4.6}$$

$$(XU)_{np} = \sum_{s=1}^S Z_{nsp}; Z_{nsp} \sim \text{Poisson}(H_{ns}W_{sp}); \text{with } H_{ns}, W_{sp} \geq 0; \sum_{p=1}^P W_{sp} = 1 \tag{3.4.7}$$

$$\tilde{H}_{ns} \sim \text{Gamma}(a_H, b_H); \tilde{W}_{sp} \sim \text{Gamma}(a_W, b_W); \text{ then normalize} \tag{3.4.8}$$

$$W_{sp} = \tilde{W}_{sp} / \sum_{p'=1}^P W_{sp'}; H_{ns} = \tilde{H}_{ns} \sum_{p'=1}^P W_{sp'}; \text{ so that } H_{ns}W_{sp} = \tilde{H}_{ns}\tilde{W}_{sp}.$$

In above $A_{\bullet,r}$ denotes the r -th column of a matrix A . Below we discuss the model in detail.

3.4.1 Multi-logit regression and generalized odds ratios

The two topmost layers (3.4.1) and (3.4.2) above are similar to the original hidden genome model. The model uses a symmetric multi-logistic representation (Friedman, Hastie, and Tibshirani 2010) that allocates a regression coefficient to each variant j and cancer site k . The model is *not* likelihood identified and it requires the subsequent layers for estimability of the regression parameters. Post-estimation interpretation of the parameters can be made through a post-hoc constraint, e.g., $\sum_{k=1}^K \beta_{jk} = 0$ for each j . Then β_{jk} measures the “one-vs-all” log *generalized* odds ratio of classifying into the k -th cancer type relative to *all* K sites, given a one-unit change only in the *proportion of mutations* at variant j (Zahid and Tutz 2013). Other types of generalized odds ratios, including “one-vs-one” (i.e., the usual baseline model odds ratios) and “one-vs-rest” odds ratios, can also be derived from $\{\beta_{jk}^0\}$, $\{\theta_{sk}\}$, and $\{\omega_{pk}\}$; see Supplement A for more details.

3.4.2 Observed and topic meta-feature regression

The layer (3.4.3) expresses the *observed meta-feature* regression coefficients $\{\omega_{pk} : p = 1, \dots, P\}$ as linear combinations of *topic-meta feature regression coefficients* $\{\theta_{sk} : s = 1, \dots, S\}$ corresponding to S latent topics ($S < P$; often $S \ll P$; see the note in Supplement B). Here $W^{-} = W^T(WW^T)^{-1}$ so that $WW^{-} = I_S$, the S dimensional identity matrix. This construct induces a unique $\omega_{\bullet,k}$ satisfying $W\omega_{\bullet,k} = \theta_{\bullet,k}$ in that for any other $\tilde{\omega}_{\bullet,k}^*$ satisfying $W\tilde{\omega}_{\bullet,k}^* = \theta_{\bullet,k}$ we may recover $\omega_{\bullet,k}$ by projecting $\tilde{\omega}_{\bullet,k}^*$ on the row space of the topic matrix W : $\omega_{\bullet,k} = W^T(WW^T)^{-1}W\tilde{\omega}_{\bullet,k}^* = \mathcal{P}_{WT}\tilde{\omega}_{\bullet,k}^*$ where \mathcal{P}_{WT} denotes the projection matrix on the column space of W^T or equivalently on the row space of W . Furthermore, since each row of W is a categorical probability measure embodying a topic, $\theta_{s,k}$ can be interpreted as *the expected/average* value of the observed meta-feature regression coefficients $\{\omega_{p,k} : p = 1, \dots, P\}$ with respect to the s -th topic $\{W_{sp} : p = 1, \dots, P\}$. The connection (3.4.3) aids quantification of regression coefficients associated with both observed meta-feature categories and latent meta-feature topics in the model. This is in contrast to virtually every existing supervised topic model in that they only aid quantification for the latter; in genomic applications the former may also be of relevance (see the example in Section 4.2). Note that $\{\omega_{pk}\}$ can be derived post-hoc;

for implementation one focuses only on $\{\theta_{sk}\}$ which aids substantial dimension reduction over $\{\omega_{pk}\}$.

3.4.3 Hierarchical group-lasso prior on the independent regression coefficients

The hierarchical group lasso prior (Kyung et al. 2010) layer (3.4.5) assigned on the *independent* regression coefficients $\{\beta_{jk}^0, \theta_{sk}\}$ encourages group-wise shrunken estimation of these parameters. Here each group is constituted by the K coefficients across all cancer sites for a variant j or a meta-feature topic s . Because the corresponding columns of \tilde{X} or $\tilde{X}UW^-$ have different scales, the group lasso prior is considered on coefficients *scaled* by the corresponding column sample standard deviations (denoted as $\hat{\text{sd}}(\cdot)$ and evaluated from the N data points). Note that the sample standard deviations of the columns of $\tilde{X}UW^-$ involve model parameters W , and hence this scaling cannot be done simply as data pre-processing. In the proposed MCMC sampler for the model this is done once per iteration; see Section 3.5 and supplement A for more details on implementation of the model. To aid Bayesian estimation of the group-lasso sparsity parameter λ , a Gamma(a_λ, b_λ) prior is considered for λ^2 on layer (3.4.4) (Kyung et al. 2010). When knowledge on the sparsity level is lacking a vague prior induced, e.g., by $a_\lambda = 0.01$ and $b_\lambda = 0.01$ can be used. Note that intercepts $\{\alpha_k\}$ are not shrunken; they are assigned a fixed, non-hierarchical $\text{N}(0, \tau_{0,\alpha}^2)$ prior in layer (3.4.4). A moderately large $\tau_{0,\alpha}$ (e.g., $\tau_{0,\alpha} = 10$) is suggested to make the prior weakly informative.

3.4.4 Topic model for observed meta-feature categories

The layer (3.4.7) induces a topic model over the P observed meta-feature categories. To see this, consider tumor $n \in \{1, \dots, N\}$ with total mutation burden M_n of which $V_{np} = (XU)_{np}$ associates with the meta-feature category $p \in \{p = 1, \dots, P\}$. The quantities $\{Z_{nsp}\}$ measure *latent contributions* of the s -th topic ($s = 1, \dots, S$; $S < P$) to the count V_{np} and aid conjugacy for MCMC sampling (Supplement C; also see Liang and Hoffman (2014)). It follows that $V_{np} \sim \text{Poisson}(\sum_{s=1}^S H_{ns}W_{sp})$ and conditional on $M_n = \sum_{p=1}^P V_{np}$, $(V_{n1}, \dots, V_{nP}) \sim \text{Multinomial}_P(M_n; (\sum_{s=1}^S \zeta_{ns}W_{s1}, \dots, \sum_{s=1}^S \zeta_{ns}W_{sP}))$ where $\zeta_{ns} = H_{ns} / \sum_{p=1}^P \sum_{s'=1}^S H_{ns'}W_{s'p} = H_{ns} / \sum_{s'=1}^S H_{ns'}$. Equivalently, $(V_{n1}, \dots, V_{nP}) \sim \sum_{s=1}^S \zeta_{ns}f_s$ where $f_s \equiv \text{Multinomial}_P(M_n; (W_{s1}, \dots, W_{sP}))$. Define topic- s through the *composition probabilities* (W_{s1}, \dots, W_{sP}) . Then f_s is the probability distribution of allocations assigning M_n mutations into P meta-feature categories following the composition probabilities of topic- s , and ζ_{ns} is understood as the *exposure* to topic- s in tumor n .

We make a few notes here. First, (3.4.7) can be interpreted as a parametric formulation of non-negative matrix factorization (NMF) $V \approx HW$ (Paisley, Blei, and Jordan 2014) commonly used for mutation signature estimation in genomics. Second, the parameters H and W are not identified. This makes subsequent inference on them challenging. This is a well-known problem in topic modeling and mixture models in general; in Section 3.8 we discuss a simple clustering-based approach to this problem. Finally, the topic model hyper-parameters, namely $a_H, b_H; a_W, b_W$; and S all need to be judiciously chosen. A detailed discussion on these parameters is provided in the Supplement

B. In our experiments we found small values such as $a_H = b_H = 1$ and $a_W = b_W = 0.5$ and a moderately large S between 50 to 75 to produce models balancing predictive ability, interpretability, and computational costs.

3.5 Full Bayesian Implementation via MCMC

The posterior distribution for the proposed model is highly intractable. For implementation we propose a doubly data augmented, blocked, *independence* Metropolis-within-Gibbs algorithm for MCMC sampling from the target posterior. We provide a summary of the algorithm below; a detailed description with notes on initialization is provided in Supplement A. We note that to aid computation, prior to using the MCMC sampler one needs to screen the columns of the training predictor matrix \tilde{X} *after* computing the product matrices XU and $\tilde{X}U$. This effectively amounts to setting the residual effects $\{\beta_{jk}^0\}$ to be zero *a priori* for all but a few (say ≤ 50) highly discriminating variants $\{j\}$. Following Chakraborty, Begg, and Shen (2020) we use a computationally efficient mutual information based variable screening for this.

The proposed Gibbs-type MCMC algorithm iteratively draws (a) topic model parameters, and (b) group-lasso multi-logistic parameters in two blocks each containing a separate data-augmentation step. In block (a) latent Poisson data $\{Z_{nsp}\}$ (Liang and Hoffman 2014) are augmented to aid MCMC sampling of (H, W) . To account for the *supervised* contribution of the multi-logistic layer we propose an *independence* Metropolis-Hastings step that *requires no manual tuning*. In block (b) a Gibbs draw is performed for the hierarchical group-lasso (Kyung et al. 2010) multi-logistic parameters with a *column-scaled* $(\tilde{X}, \tilde{X}UW^-)$ used as predictor matrix (see Chakraborty, Begg, and Shen 2020). Conditional conjugacy for the multi-logistic parameters are achieved via Pólya-Gamma data augmentation (Polson, Scott, and Windle 2013).

3.5.0.1 Approximations While exact MCMC sampling along the steps above is theoretically possible, it is still too computation-intensive to be practicable in sizable applications. Fortunately, substantial computational gains are achieved via a *first order Taylor* approximation resembling the usual NMF assumption $V_{np} \approx E(V_{np} | \{H_{ns}, W_{sp}\}) = \sum_{s=1}^S H_{ns}W_{sp}$ (Lee and Seung 1999) inside the Metropolis-Hastings acceptance probability for block (a). A second approximation to encourage better mixing is made by assuming that the change in the standard deviation terms $\{\tilde{\sigma}_{\text{topic},s}\}$ due to a change in H (Metropolis Hastings proposal vs. current values). Together, these permit approximate, but efficient independent drawing of the elements of W given H and the rows of H *given* W (see Supplement A).

3.6 Handling multiple, possibly continuous, meta-feature sources

To handle multiple categorical meta-feature sources, one may introduce into the model separate, independent topic model layers (3.4.7)-(3.4.8) and a topic-to-observed coefficient connection layer (3.4.3) for each source. Continuous meta-feature sources, if present, would directly produce observed

meta-feature regression coefficients ω . All *observed* meta-feature regression coefficients are then stacked for use in layer (3.4.2). The MCMC algorithm discussed in Section 3.5 requires small modifications to reflect these new layers. With several categorical meta-feature sources one would sequentially update the topic parameters for each source conditional on the “supervised” multi-logistic contributions of the other source topics. The hierarchical group-lasso multi-logistic regression is performed on an expanded column scaled predictor matrix column-stacking X , all $\tilde{X}UW^-$ matrices arising out of categorical meta-feature sources, and all XU matrices arising out of continuous sources.

3.7 Bayesian Posterior Predictive Probabilities

A full Bayesian “ensemble” prediction using posterior MCMC draws $\{\alpha^{(t)}, \beta^{0,(t)}, \omega^{(t)} : t = 1, \dots, T\}$ for the multi-logistic parameters is described as follows. Given a “new”/test tumor with *normalized* variant indicators \tilde{x}_{new} , one first finds variants $\{j\}$ in \tilde{x}_{new} with non-zero residual effects $\{\beta_{j,k}^{0,(t)} : k = 1, \dots, K\}$ for each draw $t = 1, \dots, T$. All remaining variants $\{j^*\}$, including “novel” variants in test data and screened out variants in training data are assigned $\{\beta_{j^*,k}^{0,(t)} = 0 : k = 1, \dots, K\}$. The meta-feature values u_{j^*} for a “novel” variant j^* are cataloged as a new row of U for computation of $\tilde{x}_{\text{new}}^T U$. Subsequently, for each draw $t \in \{1, \dots, T\}$ one computes first the linear predictions using the layers (3.4.1) and (3.4.2): $\{\eta_k^{(t)} = \alpha_k^{(t)} + \tilde{x}_{\text{new}}^T \beta^{0,(t)} + \tilde{x}_{\text{new}}^T U \omega^{0,(t)} : k = 1, \dots, K\}$ for all K cancer sites. These draw-specific linear predictions are then “softmax”-ed and subsequently averaged across draws to compute cancer-site specific posterior predictive probabilities:

$$\begin{aligned} & \Pr(c_{\text{new}} = k \mid x_{\text{new}}, \text{training data}) \\ &= \int \Pr(c_{\text{new}} = k \mid \alpha, \beta^0, \omega, \tilde{x}_{\text{new}}, \text{training data}) \pi(\alpha, \beta^0, \omega \mid \text{training data}) d(\alpha, \beta^0, \omega) \\ &\stackrel{\text{computed}}{=} \frac{1}{T} \sum_{t=1}^T \Pr(c_{\text{new}} = k \mid \alpha^{(t)}, \beta^{0,(t)}, \omega^{(t)}, x_{\text{new}}, \text{training data}) = \frac{1}{T} \sum_{t=1}^T \frac{\exp(\eta_k^{(t)})}{1 + \exp(\eta_k^{(t)})}. \end{aligned}$$

Note that unlike a point estimate-based prediction (e.g., MAP prediction) the above acknowledges model estimation uncertainty, and is thus preferred in full Bayesian inference.

3.8 Inference on the latent signatures: post-hoc identification via clustering

The topic related parameters W , H , and $\{\theta_{sk}\}$ may reveal important biological insights. However, their estimation is challenging due to their non-identifiability caused by the mixture structure of the topic model. Directly using MCMC outputs for these parameters for point/interval estimation may produce misleading results.¹ Instead, using a point process representation of MCMC draws (Frühwirth-Schnatter 2011), we introduce a simple clustering approach to post-hoc identification and approximate inference for these parameters.

¹Note only direct inference on the (topic) parameters H , W , and $\{\theta_{sk}\}$ is challenging. Inference on posterior quantities that marginalizes over these parameters, e.g., prediction for new data and estimation of $\{\beta_{jk}^0\}$ and $\{\omega_{pk}\}$ is straightforward.

Briefly, we first create a list of all topics (the rows of W) drawn across all iterations of the MCMC run, and cluster these pooled rows using k -means with an appropriately chosen k (via elbow method in our computations). The key idea is then to use the consequent cluster assignments to relabel MCMC draws for the topics (rows of W), topic exposures (columns of H) and topic regression coefficients $\{\theta_{sk}\}$. These cluster-relabeled draws are then treated as posterior MCMC draws for “post-hoc identified” parameters and used for MCMC output-analysis as usual. We make a few notes on the use of k -means as a clustering algorithm in the current context. First, a pairwise distance based clustering algorithm, e.g., k -medoids, might be conceptually preferable to k -means given the simplex nature of the topics. However they are not practicable when the number of topics S and/or the number of MCMC iterations T is even moderately large. Second, k -means results are sensitive to outliers. Here outliers correspond to posterior draws for the rows of W that are far from any other rows of W drawn in any iteration, and hence may represent configurations with low posterior probabilities. To avoid the influence of these outliers, we considered an approximate nearest neighbors-based filtering prior to k -means clustering. Finally, k means algorithm suffer from high computational expense and reduced stability as the number of meta-feature categories (number of columns of W) grows. This is particularly challenging for gene and window meta-feature sources with hundreds to thousands of categories. To manage the computation load, prior to k -means (and outlier detection) we perform PCA and retain the first few (50 in our computations) principal components.

The above approach resembles the k -means finite mixture model identification approach of Frühwirth-Schnatter (2011). However, instead of only resolving label-switching/permutation modes as done in finite mixtures here we use clustering to also possibly combine duplicated topics/modes arising *within the same MCMC iteration*. Furthermore, while heuristic, Bayesian estimation via “cluster identified” MCMC draws may still be viewed as an approximate solution to a rigorously defined decision theoretic problem; see Stephens (2000).

4 Data Example

We implement the proposed model on the full PCAWG whole genome data with $K = 10$ sites, and its restricted whole exome and targeted cancer gene panel subsets. On the whole genome set we consider three discrete meta-feature sources: gene, SBS, and 1-MB chromosome windows. For the simulated subsets where chromosome windows trace only the gene level mutations, we consider two sources: gene and SBS. For each source we set $S = 50$. The models are then fitted using the proposed MCMC algorithm using marginal MAP (for α , β^0 , and ω) and unsupervised NMF (for H and W) based initialization of parameters as described in Supplement D. On each dataset the MCMC algorithm is run for 20,000 iterations after discarding the initial 1000 iterations as burn-in. For compute and memory feasibility, we updated the topic model parameters H and W once every 10-th iterations while updating all other parameters at every iteration; these 10-th iterations are then stored (*thinning*) and subsequently used for Bayesian estimation and prediction.

4.1 Predictive performance under cross validation

On each dataset, we perform 10 fold cross-validations to assess predictive performance of the model. The folds are created using stratified (based on cancer sites) random partitions of the PCAWG tumors; these produce 10 different training/test set combinations obtained by pooling each 9 of the 10 folds for training and the remaining fold for testing. On each training set a separate model is fitted and then used for Bayesian (posterior) prediction of the corresponding test set. The predicted class probabilities for all tumors in all folds are subsequently combined. To aid comparison, alongside we also obtain analogous MAP predictions from the hidden genome model (without any topics) of Chakraborty, Begg, and Shen (2020) with similar normalized \tilde{X} as predictors. For each model, we derive one-vs-rest classification probabilities for each of the $K = 10$ cancer sites, and compute the associated area under the one-vs-rest precision-recall curve (PR AUC) as a measure of site-specific predictive performance (Saito and Rehmsmeier 2015). PR AUCs reflect class-size imbalances, and are more informative than ROC AUCs for one-vs-rest comparisons obtained from a multi-class classifier. The site-specific PR AUCs are then averaged to produce an overall metric for each model. We consider 10 random replications of this cross-validation, and obtain model specific average PR AUCs across replications. These average PR AUCs are displayed as barplots in Figure 1 with results from the three different subsets plotted along panels. The figure also shows the *null baseline* PR AUC value for each site, corresponding to a *null* classifier randomly assigning observations to classes. The null baseline PR AUCs are proportional to the sample size of the corresponding class (see Chakraborty, Martin, et al. (2021)).

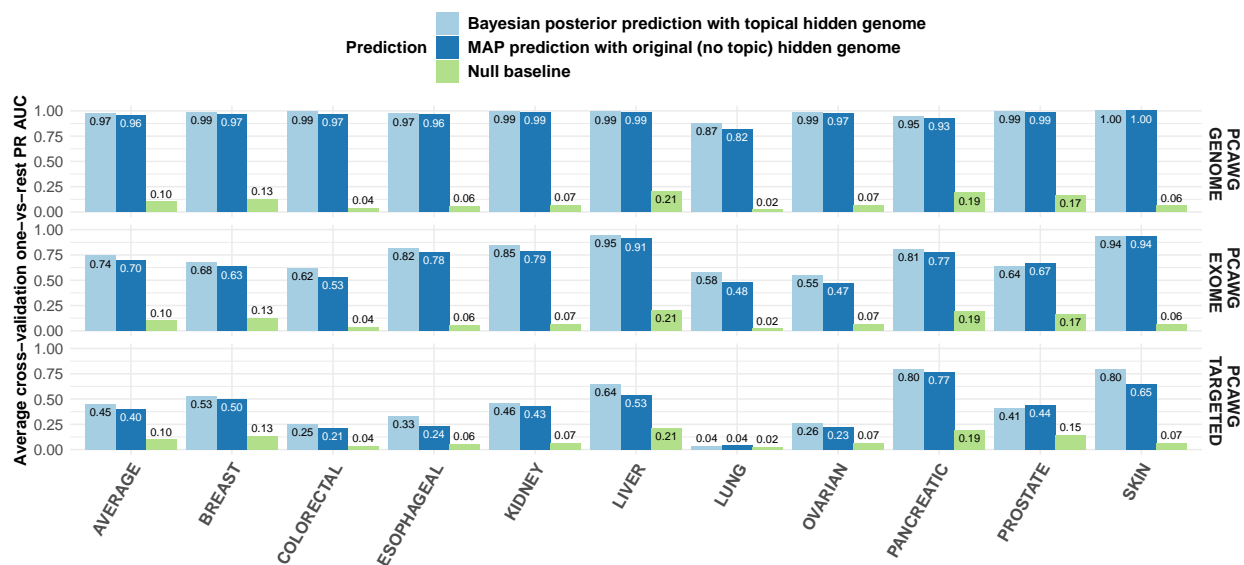


Figure 1: Comparing cross-validation PR AUC (averaged across 10 independent cross validations) of the original hidden genome model (without topics) MAP predictions and proposed topical hidden genome posterior predictive probabilities. The null baseline corresponds to a classifier that randomly assigns cancer site labels to tumors

We make the following observations from Figure 1. First, the full Bayesian prediction from the proposed model has a better overall-level performance than the MAP prediction from the original model. The improvement is most prominent in targeted gene panel data followed by exome level and whole genome level data. This overall improvement is likely due to the topic model-based dimension reduction which facilitates more stable estimation and prediction. Second, all except one cancer site demonstrate improvement in site-specific prediction in the proposed model. Certain cancer sites, such as lung and pancreas, show consistently better prediction in all three datasets; while for certain other sites, notably skin cancer in targeted gene sequencing, the improvement is noticeable only at specific subsets. Third, for only one site, namely prostate, is there a drop in PR AUC in the proposed approach. This indicates the lack/non-existence of discriminative topics for prostate cancer, which is known to have a rather sporadic mutational landscape. However, the nominal drop in prostate is more than compensated by improvements in the other sites, making the proposed approach superior to the hidden genome model of Chakraborty, Begg, and Shen (2020) as a predictive model.

4.2 Bayesian inference on tissue-specific topics and meta-features and validation of results

This section illustrates how to make inference from the proposed model through its applications on the PCAWG datasets. For brevity here we focus on the full whole genome and the exome-subsetted datasets; analogous inferences can also be drawn on the targeted cancer gene panel subsets. Using the proposed MCMC algorithm we fit our model to each dataset similarly as discussed in Section 4.1, except now we use the full datasets instead of cross-validation partitions to train the models. Subsequently in each dataset we compute point (posterior mean and median) and 80% (highest posterior density) interval estimates of topic model parameters and one-vs-rest log odds ratio parameters obtained from regression coefficients for latent meta-feature topics, observed meta-feature categories, and residual variant effects, using the MCMC draws for model parameters.

Tissue-specific window topics in PCAWG whole genome data. We first focus on the whole genome dataset. It is known (Jiao et al. 2020; Chakraborty, Martin, et al. 2021) that whole genome mutation densities at 1-MB chromosome windows collectively aid near perfect classification of tumor types, and so we obtain the estimated latent window topics and their log odds ratios. Several highly tissue-specific latent topics are obtained from the model with strikingly high log-odds ratios. For exposition here we focus on one, a liver cancer specific topic displayed on Figure 2. It is known that somatic mutational landscape in the cancer genome is shaped by the epigenome structure of the corresponding site of origin (Polak et al. 2015). For example, regions enriched for transcription regulatory elements (e.g., histone marks) are observed to have low somatic mutation rates. Indeed, a major pattern emerged from our analysis of the whole-genome is that the variation of mutation density across the genome can be explained to a high degree by site-specific epigenome organization. Specifically, we compare the estimated composition probabilities for this topic at each individual

chromosome window with an associated epigenomic histone score H3K4me1 obtained from cells sequenced in an independent study cohort (Dunham et al. 2012) separately for each of the 10 sites. Interestingly, these topic composition probabilities have a moderately strong negative association with liver cell-specific epigenomic features (Spearman $\rho \approx -0.6$; Figure 2C; a negative correlation indicates that regions enriched for regulatory elements have low observed somatic mutation density), but only small associations with other site-specific epigenome features (Spearman $\rho \leq 0.46$ in absolute values; see Figure S1 in Supplement E). This implies that this topic may explain the epigenomic landscape of liver tumors, and is thus biologically relevant for characterizing liver cell of origin.

Tissue-specific estimated SBS topics from PCAWG-exome data and assessing their reproducibility with estimates from TCGA-exome data and results from the literature.

We next focus on the model trained on the PCAWG exome subsetted data, and obtain estimates for the SBS topics and the corresponding tissue-specificities as quantified by the odds ratios. As noted before, much research has been done on SBS signatures (analogous to topics) in exome level mutation data, and several highly tissue site specific SBS signatures have been detected. This permits direct reproducibility assessment for our results. We consider (a) estimated SBS topics and odds ratios from a similar model trained on the independent TCGA exome data restricted to the same 10 cancer sites, and (b) exome level known SBS mutation signatures noted on the literature (COSMIC database; Ludmil B. Alexandrov et al. (2020))² as a biological benchmark. We highlight top three discriminative PCAWG-exome estimated SBS topics with high one-vs-rest log odds ratios, and compare them with all TCGA-estimated SBS topics, and COSMIC signatures to identify the closest match for each. Here “closeness” is measured through total variation distance defined for two topic compositions (discrete probability functions) W_1 and W_2 over the same meta-feature categories $\{1, \dots, P\}$ as $TV(W_1, W_2) = \frac{1}{2} \sum_{p=1}^P |W_{1p} - W_{2p}|$. These three topics are displayed on the three panels of Figure 3. The second topic (panel B) has a very close match to the UV signature in the COSMIC database and uniquely associated with melanoma (skin). The first topic (panel A) show a pattern that clearly matches the APOBEC signature from COSMIC, but the TV distance is relatively higher suggesting this topic is a modified version of APOBEC signature. Since APOBEC exist in multiple cancer types, this difference is likely attributable to our supervised topic model contrasting a cancer-site agnostic approach used to derive the COSMIC signatures. Similarly, the third topic (panel C) shows a pattern that matches the COSMIC signature of De-amination of 5-methylcytosine (clock-like), but have relatively poorer matches in TV distance since we incorporated cancer site information in our analysis.

Tissue-specific gene topics from PCAWG-exome subsetted data. Interestingly, the gene meta-feature categories did not produce strong tissue specific latent topics, and the estimated topics showed high variability in their composition probabilities. In Figure 4 we display two gene

²The mutation signatures noted in COSMIC are derived from the TCGA data using an unsupervised NMF approach, and they collectively serve as a “baseline” for comparing our PCAWG-estimated SBS topics.

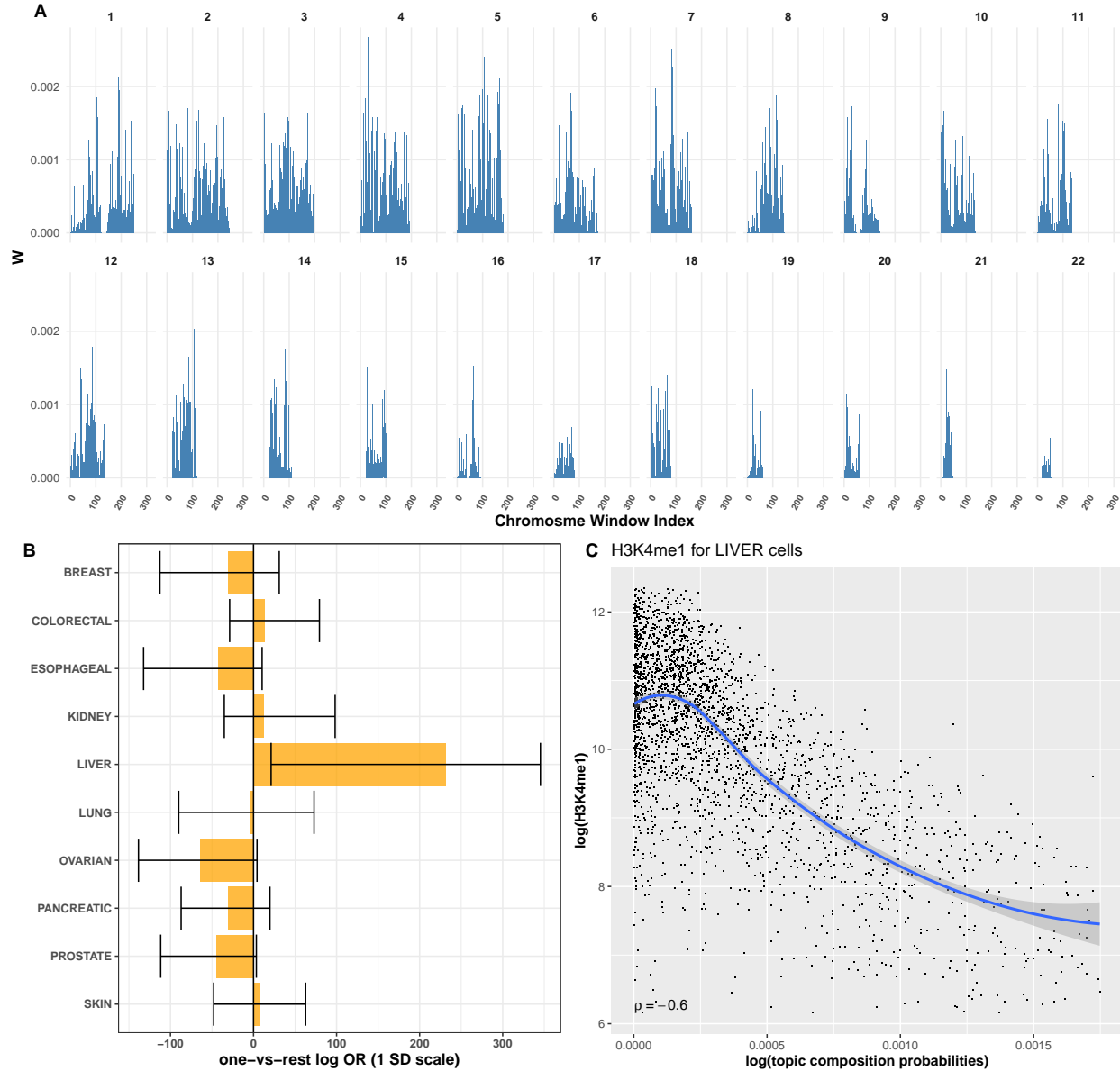


Figure 2: Inferring a liver cancer specific chromosome window topic estimated from the PCAWG data, and understanding its tissue site specificity and interpretability. **Panel A:** The blue vertical bars quantify posterior mean topic composition probabilities across ~ 3000 chromosome windows grouped by the chromosome numbers. **Panel B:** The orange horizontal bars and the black whiskered lines visualize posterior medians and 80% HPD intervals for the cancer site-specific one-vs-rest log odds ratios, calculated for one standard deviation increase in the total fraction of mutation burden attributable to the topic. **Panel C:** Points in the scatter display the log composition probabilities for the topic along the x-axes and log epigenomic features (histone marks H3k4me1) for liver cells along the y-axes for all ~ 3000 chromosome window meta-feature categories. Inscribed at the bottom-left corner of the panel is the Spearman correlation coefficient ρ between the corresponding topic composition probabilities and H3k4me1 scores.

topics with the largest median site specific one-vs-rest log ORs. Both topics are strongly driven by TP53 and KRAS, although the composition probabilities vary substantially (vertical error bar over the bars). Furthermore, for all cancer sites, the 80% CIs for the log ORs (horizontal whiskers on the right panels) span almost entirety of (-0.5, 0.5), indicating the lack of tissue-site specificity of these topics. Together these likely indicate that the tissue-specific genes do not mutate in unison, unlike the chromosome windows and SBS categories.

Inferring tissue specificities of residual variants and "observed" meta-features. Finally, we focus on individual variant-specific *residual* effects and "observed" meta-feature category effects. We consider the exome level PCAWG data, and obtain component wise one-vs-rest log odds ratios from the residual variant effects β^0 and observed meta-feature category effects ω . Then we rank the individual variants and observed meta-feature categories (separately for each meta-feature source of gene and SBS) based on their maximum (posterior median) log one-vs-rest odds ratio values obtained across cancer sites. The top five predictors from each group (variants and each meta-feature source) are then selected, and the posterior median and 80% HPD intervals for their cancer site specific log one-vs-rest odds ratios are plotted as horizontal bars in Figure 5. The findings visualized in Figure 5 agree with existing scientific knowledge, and aid quantification of some interesting genomic facts. For example KRAS gene mutations is known to be associated with multiple cancer sites including pancreatic and lung; however, specific variants of KRAS, e.g., c.35C>A are more specific to only pancreatic cancer.

5 Discussion

This paper proposes a multilevel Bayesian multi-logit regression model for statistical inference in ultra-high dimensional genome driven cancer type characterization problems. The approach leverages bi-level dimension reduction for efficient, practicable MCMC-based implementation – (a) condensing information in millions of observed, sparse variants into a few thousands of observed meta-feature contexts, and then (b) modeling the effects of these observed meta-features through lower dimensional latent *meta-feature topics*. The latter is a manifestation of topic models (Blei and Lafferty 2009) that derive *interpretable* latent lower dimensional structures ("topics") from observed high-dimensional categorical data to facilitate *parts-based representation* of a complex underlying system. These models have found important applications in several scientific and engineering disciplines, including computational linguistics, genomics (particularly, mutation signature extraction; Ludmil B. Alexandrov et al. (2013); Funnell et al. (2019)), computer vision, and acoustic signal processing, among others. The usefulness of topic models in aiding interpretable lower dimensional structures has prompted its use as an interpretable dimension reduction tool for regression/classification (supervised learning) tasks, and a rich literature has been devoted to the development of supervised topic models. See McAuliffe and Blei (2007), Zhu, Zheng, and Zhang (2013), Magnusson, Jonsson, and Villani (2020) and the references therein for a review. To our knowledge, however, none of

the existing approaches integrate a topic model as an intermediate layer of an elaborate Bayesian multinomial-logistic regression model, and enable MCMC-based estimation, as proposed herein. Furthermore, our approach permits quantification of regression effects for both the observed meta-feature categories, and the latent meta-feature topics. To the best of our knowledge this is not provided by any existing supervised topic model approach; existing approaches quantify regression coefficients of the latent topics only.

The topic model layer however introduces non-identified parameters in the model, which subsequently makes statistical inference on these parameters challenging. Herein we propose a k -means based posthoc identification of the model, leveraging a point-process representation of the MCMC draws as suggested in Frühwirth-Schnatter (2011), and our results suggest reasonable practical performance of the proposed intuitive approach.

There are several future directions we aim to pursue in both methodological and applied scientific fronts. First, on the methodology side, we aim to rigorize the proposed clustering-based posthoc identification step for principled inference on the topic model parameters. Second, while not considered herein, interest may lie in allowing ‘information sharing’ between cancer sites through appropriately articulated hierarchical model layers. This may permit more coherent estimation of the tissue-specific effects of mutations. Third, a future research is planned to assess statistical performance of the model via large scale simulations. Finally, on the scientific side, we aim a thorough investigation of the tissue-specific whole genome chromosome region topics to understand their biological relevance.

References

- Alexandrov, Ludmil B., Jaegil Kim, Nicholas J. Haradhvala, et al. 2020. “The Repertoire of Mutational Signatures in Human Cancer.” *Nature* 578 (7793): 94101.
- Alexandrov, Ludmil B, Serena Nik-Zainal, David C Wedge, et al. 2013. “Signatures of Mutational Processes in Human Cancer.” *Nature* 500 (7463): 415–21.
- Bailey, Matthew H, Collin Tokheim, Eduard Porta-Pardo, Sohini Sengupta, Denis Bertrand, Amila Weerasinghe, et al. 2018. “Comprehensive Characterization of Cancer Driver Genes and Mutations.” *Cell*.
- Blei, David M., and John D. Lafferty. 2009. “Topic Models.” In: Chapman; Hall/CRC.
- Campbell, Peter J., Gad Getz, Jan O. Korbel, Joshua M. Stuart, Jennifer L. Jennings, Lincoln D. Stein, et al. 2020. “Pan-Cancer Analysis of Whole Genomes.” *Nature* 578 (7793): 82–93.
- Chakraborty, Saptarshi, Arshi Arora, Colin B. Begg, and Ronglai Shen. 2019. “Using Somatic Variant Richness to Mine Signals from Rare Variants in the Cancer Genome.” *Nature Communications* 10 (1).
- Chakraborty, Saptarshi, Colin B. Begg, and Ronglai Shen. 2020. “Using the "Hidden" genome to improve classification of cancer types.” *Biometrics*, September.
- Chakraborty, Saptarshi, Brett L. Ecker, Ken Seier, Victoria G. Aveson, et al. 2021. “Genome-

- Derived Classification Signature for Ampullary Adenocarcinoma to Improve Clinical Cancer Care.” *Clinical Cancer Research*, August.
- Chakraborty, Saptarshi, Axel Martin, Zoe Guan, Colin B. Begg, and Ronglai Shen. 2021. “Mining Mutation Contexts Across the Cancer Genome to Map Tumor Site of Origin.” *Nat. Commun* 12 (1): 3051.
- Chakravarty, Debyani, Jianjiong Gao, Sarah Phillips, et al. 2017. “OncoKB: A Precision Oncology Knowledge Base.” *JCO Precision Oncology*, no. 1 (November): 1–16.
- Dunham, Ian, Anshul Kundaje, Shelley F. Aldred, Patrick J. Collins, Carrie A. Davis, Francis Doyle, et al. 2012. “An Integrated Encyclopedia of DNA Elements in the Human Genome.” *Nature* 489 (7414): 57–74. <https://doi.org/10.1038/nature11247>.
- Efron, Bradley. 2020. “Prediction, Estimation, and Attribution.” *International Statistical Review* 88: S28S59.
- Friedman, Jerome H., Trevor Hastie, and Rob Tibshirani. 2010. “Regularization Paths for Generalized Linear Models via Coordinate Descent.” *Journal of Statistical Software* 33 (February): 1–22.
- Frühwirth-Schnatter, Sylvia. 2011. “Dealing with Label Switching Under Model Uncertainty.” In, edited by Kerrie L. Mengersen, Christian Robert, and Mike Titterton, 213239. John Wiley & Sons; Citeseer.
- Funnell, Tyler, Allen W. Zhang, Diljot Grewal, et al. 2019. “Integrated Structural Variation and Point Mutation Signatures in Cancer Genomes Using Correlated Topic Models.” *PLOS Computational Biology* 15 (2): e1006799.
- Haigis, Kevin M., Karen Cichowski, and Stephen J. Elledge. 2019. “Tissue-specificity in cancer: The rule, not the exception.” *Science (New York, N.Y.)* 363 (6432): 1150–51.
- Jiao, Wei, Gurnit Atwal, Paz Polak, et al. 2020. “A Deep Learning System Accurately Classifies Primary and Metastatic Cancers Using Passenger Mutation Patterns.” *Nat. Commun* 11 (1).
- Kyung, Minjung, Jeff Gill, Malay Ghosh, and George Casella. 2010. “Penalized Regression, Standard Errors, and Bayesian Lassos.” *Bayesian Analysis* 5 (2): 369411.
- Lapuschkin, Sebastian, Stephan Wäldchen, Alexander Binder, Grégoire Montavon, Wojciech Samek, and Klaus-Robert Müller. 2019. “Unmasking Clever Hans Predictors and Assessing What Machines Really Learn.” *Nature Communications* 10 (1): 1096. <https://doi.org/10.1038/s41467-019-08987-4>.
- Lee, Daniel D., and H. Sebastian Seung. 1999. “Learning the Parts of Objects by Non-Negative Matrix Factorization.” *Nature* 401 (6755): 788–91.
- Liang, Dawen, and Matthew D. Hoffman. 2014. “Beta Process Non-Negative Matrix Factorization with Stochastic Structured Mean-Field Variational Inference.” <http://arxiv.org/abs/1411.1804>.
- Magnusson, Måns, Leif Jonsson, and Mattias Villani. 2020. “DOLDA: A Regularized Supervised Topic Model for High-Dimensional Multi-Class Regression.” *Computational Statistics* 35 (1): 175–201. <https://doi.org/10.1007/s00180-019-00891-1>.
- Mcauliffe, Jon, and David Blei. 2007. “Supervised Topic Models.” In. Vol. 20. Curran Associates.

- <https://proceedings.neurips.cc/paper/2007/hash/d56b9fc4b0f1be8871f5e1c40c0067e7-Abstract.html>.
- Paisley, John, David M. Blei, and Michael I. Jordan. 2014. “Bayesian Nonnegative Matrix Factorization with Stochastic Variational Inference.” In. Chapman; Hall/CRC.
- Polak, Paz, Rosa Karlić, Amnon Koren, Robert Thurman, Richard Sandstrom, Michael Lawrence, et al. 2015. “Cell-of-Origin Chromatin Organization Shapes the Mutational Landscape of Cancer.” *Nature* 518 (7539): 360–64. <https://doi.org/10.1038/nature14221>.
- Polson, Nicholas G., James G. Scott, and Jesse Windle. 2013. “Bayesian Inference for Logistic Models Using Pólya–Gamma Latent Variables.” *J Am Stat Assoc* 108 (504): 1339–49. <https://doi.org/10.1080/01621459.2013.829001>.
- Saito, Takaya, and Marc Rehmsmeier. 2015. “The Precision-Recall Plot Is More Informative Than the ROC Plot When Evaluating Binary Classifiers on Imbalanced Datasets.” *PLOS ONE*, March.
- Soh, Kee Pang, Ewa Szczurek, Thomas Sakoparnig, and Niko Beerenwinkel. 2017. “Predicting Cancer Type from Tumour DNA Signatures.” *Genome Medicine* 9 (1).
- Stephens, Matthew. 2000. “Dealing with Label Switching in Mixture Models.” *Journal of the Royal Statistical Society: Series B (Statistical Methodology)* 62 (4): 795–809. <https://doi.org/10.1111/1467-9868.00265>.
- Yuan, Ming, and Yi Lin. 2006. “Model Selection and Estimation in Regression with Grouped Variables.” *J R Stat Soc Series B Stat Methodol* 68 (1): 49–67.
- Zahid, Faisal Maqbool, and Gerhard Tutz. 2013. “Ridge Estimation for Multinomial Logit Models with Symmetric Side Constraints.” *Computational Statistics* 28 (3): 1017–34. <https://doi.org/10.1007/s00180-012-0341-1>.
- Zehir, Ahmet, Ryma Benayed, Ronak H Shah, Aijazuddin Syed, Sumit Middha, Hyunjae R Kim, et al. 2017. “Mutational Landscape of Metastatic Cancer Revealed from Prospective Clinical Sequencing of 10,000 Patients.” *Nature Medicine*.
- Zhu, Jun, Xun Zheng, and Bo Zhang. 2013. “Improved Bayesian Logistic Supervised Topic Models with Data Augmentation.” *arXiv Preprint arXiv:1310.2408*.

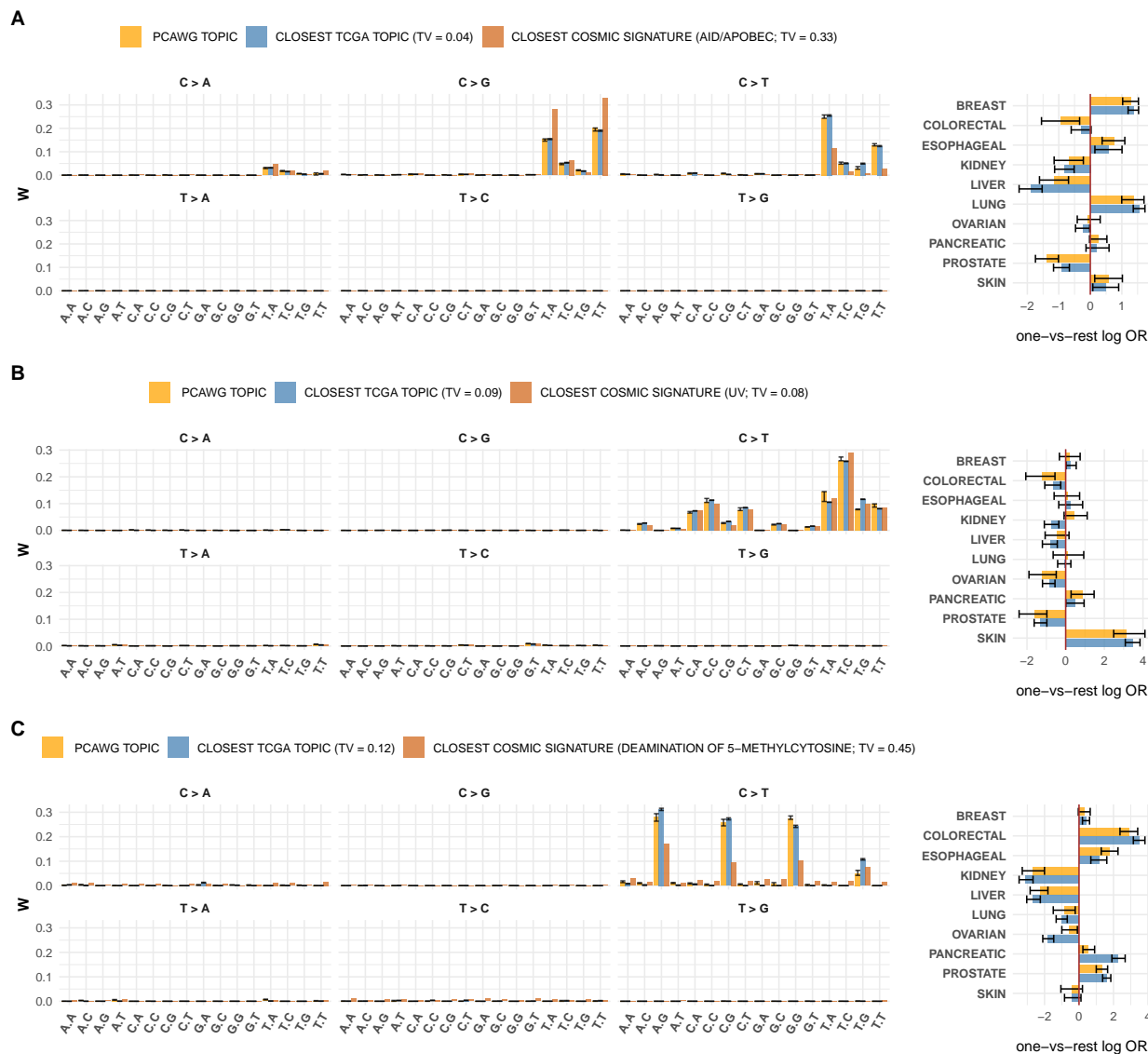


Figure 3: Inferring 3 strongly discriminative SBS topics (panels A-C) and their tissue site specificities estimated from the PCAWG data, and assessing reproducibility of the results with estimates from independent TCGA data and the COSMIC mutation signature repository. The vertical bars on the left show topic composition probabilities, estimated via posterior means for PCAWG and TCGA datasets and collected from online repository for COSMIC, across 96 SBS categories grouped by substitution types such as C>A, C>G etc. The horizontal bars on the right show estimated (via posterior median) cancer site specific one-vs-rest log odds ratios for one standard deviation increase in the total fraction of mutation burden attributable to the corresponding topic. All PCAWG estimates are displayed as orange bars. For each PCAWG estimated topic, the closest (in terms of TV distance) TCGA estimated (posterior mean) topic together with its estimated (posterior median) one-vs-rest log odds ratios are displayed through vertical and horizontal blue bars respectively, and the closest COSMIC mutation signatures are plotted as red vertical bars on the left. The names/functions of the closest COSMIC signatures are noted within parentheses in the legend. The black whiskers on each estimated bar display the associated 80% HPD credible intervals.

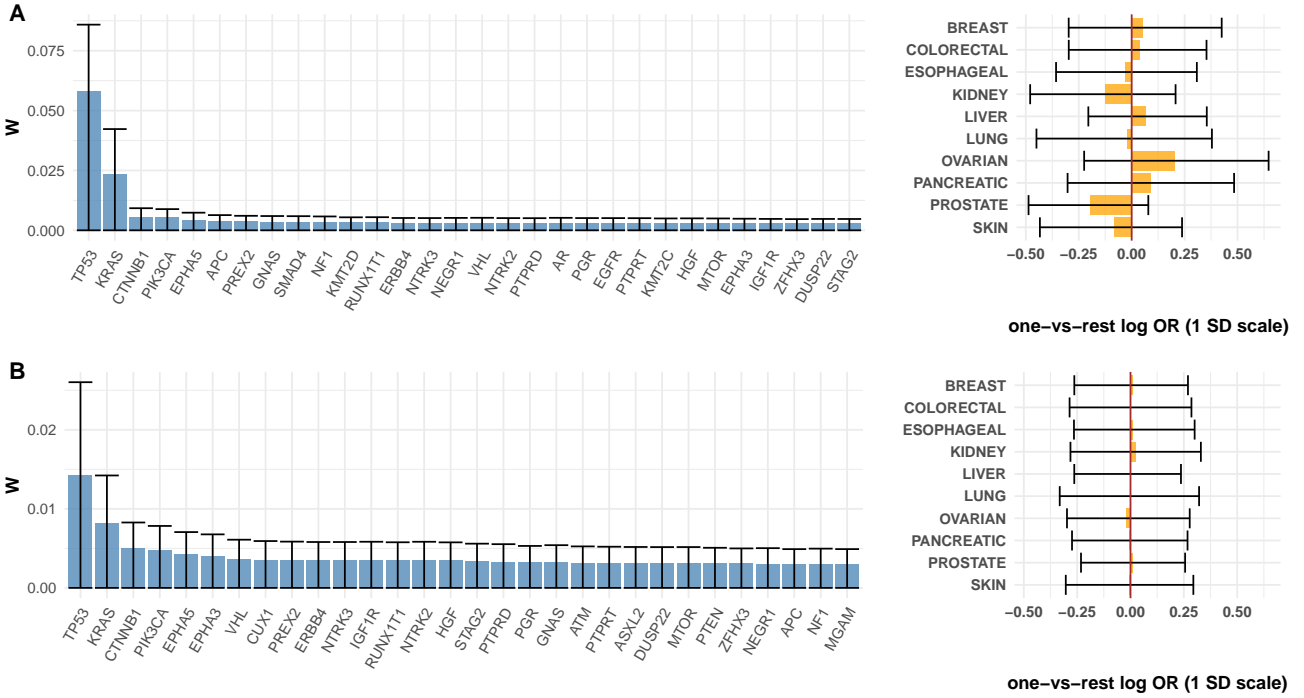


Figure 4: Inferring 2 gene topics and their tissue site specificities for PCAWG exome subsetted data. The blue vertical bars on the left quantify posterior mean topic composition probabilities for 30 most prominent genes in the topic, and the black vertical error-whisker bars show associated 80% HPD intervals for the weights. The orange horizontal bars and the black whiskered lines on the right visualize posterior medians and 80% HPD intervals for the cancer site-specific one-vs-rest generalized odds ratios, calculated for one standard deviation increase in the total fraction of mutation burden attributable to the corresponding topic.

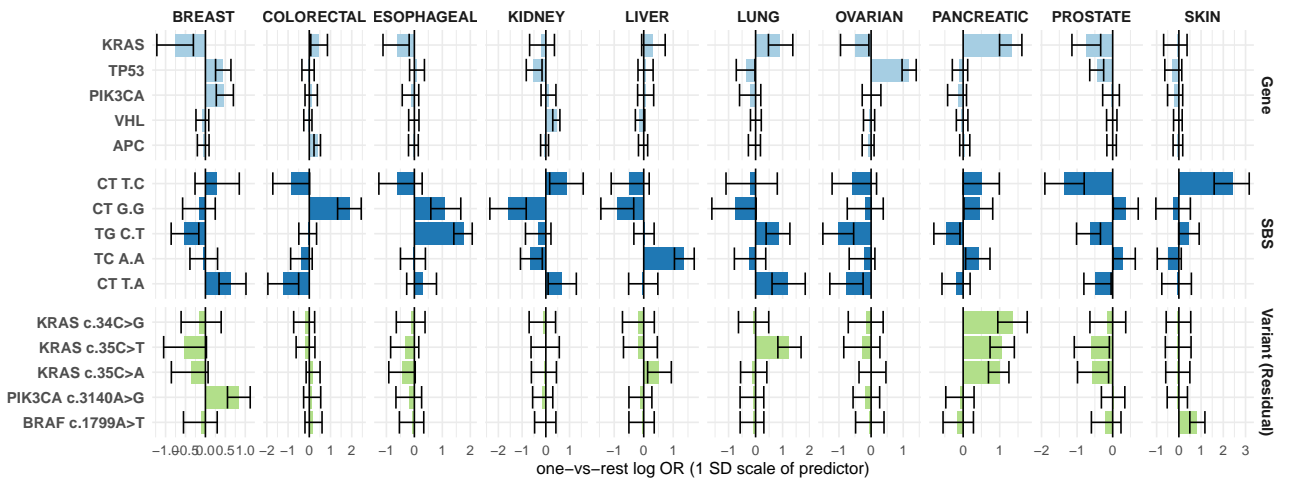


Figure 5: Inferring tissue site specificities attributable to observed meta-feature categories, and residual variant effects. The horizontal bars and the black whiskered lines visualize posterior medians and 80% HPD intervals for the cancer site-specific one-vs-rest generalized odds ratios, calculated for one standard deviation increase in the total fraction of mutation burden attributable to each meta-feature category or each individual variant.

Supplemental Information for “Topical Hidden Genome: Discovering Latent Cancer Mutational Topics using a Bayesian Multilevel Context-learning Approach”

Saptarshi Chakraborty* Zoe Guan† Colin B. Begg‡ Ronglai Shen§

A Different types of generalized odds ratios with generalized baseline categories derived from the symmetric multinomial logistic model

The generalized odds for a cancer site k given the baseline of *all cancer sites* $\{1, \dots, K\}$ is defined as

$$\text{odds}(\{k\} \mid \{1, \dots, K\}) = \Pr(c = k) / \left\{ \prod_{k'=1}^K \Pr(c = k') \right\}^{1/K}.$$

More generally, for a class $A \subseteq \{1, \dots, K\}$ of cancer sites of primary interest and a set $B \subseteq \{1, \dots, K\}$ of baseline cancer sites, we may define the generalized joint odds of the set A relative to the baseline set B as

$$\text{odds}(A \mid B) = \left\{ \prod_{k \in A} \Pr(c = k) \right\}^{1/\#(A)} / \left\{ \prod_{k \in B} \Pr(c = k') \right\}^{1/\#(B)} = \left\{ \prod_{k \in A} \text{odds}(\{k\} \mid B) \right\}^{1/\#(A)}$$

where $\#(A)$ denotes the cardinality of A . Then

$$\frac{1}{\#(A)} \sum_{k \in A} \beta_{jk} - \frac{1}{\#(B)} \sum_{k' \in B} \beta_{jk'}$$

*Department of Biostatistics, State University of New York at Buffalo, chakrab2@buffalo.edu

†Department of Epidemiology & Biostatistics, Memorial Sloan-Kettering Cancer Center, guanz@mskcc.org

‡Department of Epidemiology & Biostatistics, Memorial Sloan-Kettering Cancer Center, beggc@mskcc.org

§Department of Epidemiology & Biostatistics, Memorial Sloan-Kettering Cancer Center, shenr@mskcc.org

would measure the log-ratio of changes in $\text{odds}(A | B)$ for an analogous one unit change in the predictor value of variant j . Note that by choosing B to be the set of one specific cancer site say “1” we obtain joint odds ratios relative to cancer site “1”. On the other hand for each cancer site k , choosing $A = \{k\}$ and $B = \{1, \dots, K\} \setminus \{k\}$ provides the one-vs-rest generalized odds for site k .

Analogous generalized odds ratio-based interpretations are obtained for an observed meta-feature category p through coefficients $\{\omega_{pk}\}$, and a meta-feature topic s through coefficients $\{\theta_{sk}\}$; the odds ratios are here measured for one unit change in the proportion of total mutation burden attributable to the corresponding (topical) meta-feature category.

B The roles of hyperparameters in the topic model priors

Priors for the topic model parameters play important roles in determining the distinctness and specificity of the produced topics in individual tumors. At the outset we note that we work with the non-normalized versions \tilde{H} and \tilde{W} of the topic model parameters that satisfy $\tilde{W}_{sp} \in (0, \infty)$ with $H_{ns}W_{sp} = \tilde{H}_{ns}\tilde{W}_{sp}$ and assign gamma priors on them for analytical tractability in the proposed MCMC sampler. However, our interest lies in the normalized versions $\{H_{ns}\}$ or more specifically $\{\zeta_{ns}\}$ (tumor specific topic exposures) and

$$\{W_{sp} = \tilde{W}_{sp} / \sum_{p=1}^P \tilde{W}_{sp}\}$$

(topic specific meta-feature category weights); the prior rate parameters b_H and b_W do not have any apriori impact on these quantities and we hence may use a simpler choice, e.g. $a_H = b_H$ and $a_W = b_W$. Note that these gamma priors induce $\text{Dirichlet}_S(a_H 1_S)$ and $\text{Dirichlet}_P(a_W 1_P)$ priors on $\{\zeta_{ns}\}$ and $\{W_{sp}\}$ respectively where Dirichlet_R denotes an R component Dirichlet distribution and 1_R is the R component vector of all ones.

Leveraging the consequent analogy with the Latent Dirichlet Allocation (LDA) mixed-membership model (Blei, Ng, and Jordan 2003), it follows that a smaller (larger) value of $a_H > 0$ effectuates smaller (larger) mixing weights for most topics within a tumor, making each tumor exhibit fewer (more) topics with non-trivial exposures. On the other hand a smaller (larger) value of $b_H > 0$ makes each topic assign smaller (larger) weights to most meta-feature categories, thus making each individual topic more (less) specific to particular meta-feature categories, and thus more (less) distinct. Because our interest lies in obtaining

meta-feature topics that are as distinct (uncorrelated) and as tissue site specific as possible for interpretable inference, we prefer smaller values of a_H and b_H . However, too small values of a_H and b_H may produce topics that are entirely specific to individual tumors and are driven by only a few individual meta-feature categories. This in turn may result in poor predictive ability of the model and/or require a large number S of topics to capture all tissue-specific information in all observed meta-feature categories – a situation that curtails the computational gain achieved through the dimension reduction by signaturization. In theory, one may impose some priors on a_W and b_W to let them estimate from the data subject to some cost (loss) function balancing interpretability and predictive ability and number of topics. However, this will require additional computation-heavy steps in the proposed Gibbs sampler, and care must be taken while defining an appropriate cost function. We leave this direction as a potential future work and instead consider a reasonable fixed a_H, b_H setting in the current paper. In all our test applications across datasets the choice $a_H = b_H = 1$ and $a_W = b_W = 0.5$ provided a reasonable balance between interpretability and predictive ability of the model, and are thus used as fixed prior in this paper.

The second hyper-parameter in the topic model that requires pre-specification is the number of topics S . To this, as rule of thumb, we suggest setting S to some moderately large number such as an integer between 50 to 75 (per meta-feature source) in applications with $< 10,000$ tumors and < 20 cancer sites. However, in applications with a larger number of tumors and/or cancer sites, a larger S may be required for adequate model fit.

C Details for the MCMC sampler for posterior sampling from the full model

This section describes an MCMC sampling scheme for approximate sampling from the model posterior distribution. At the outset, first note that the normalized topic model parameters H and W are simple linear transformations of the un-normalized topic model parameters $H = \tilde{H}D_{\tilde{W}}$ and $W = D_{\tilde{W}}^{-1}\tilde{W}$ where $D_{\tilde{W}} = \text{Diag}(\sum_{p=1}^P \tilde{W}_{1p}, \dots, \sum_{p=1}^P \tilde{W}_{Sp})$. This implies,

$$W^{-} = W^T(WW^T)^{-1} = \tilde{W}^T D_{\tilde{W}}^{-1} \left(D_{\tilde{W}}^{-1} \tilde{W} \tilde{W}^T D_{\tilde{W}}^{-1} \right)^{-1} = \tilde{W} (\tilde{W} \tilde{W}^T)^{-1} D_{\tilde{W}} = \tilde{W}^{-} D_{\tilde{W}},$$

and hence $XUW^{-} = VW^{-} = V\tilde{W}^{-}D_{\tilde{W}}$ (arises in the multinomial logistic likelihood). Therefore, for posterior sampling we may focus on the unnormalized topic model parameters \tilde{H} and \tilde{W} entirely along with the other model parameters, and derive the the normalized topic model parameters H and W posthoc via transformations. The joint posterior density

of all model parameters given the observed data is as follows:

$$\begin{aligned}
& \pi(\alpha, \beta^0, \theta, \lambda^2, \{\tau_l^2\}, \{\tilde{H}_{ns}\}, \{\tilde{W}_{sp}\}, | X, XU, c) \\
& \propto \prod_{n=1}^N \left(\frac{\exp \left[\alpha_{c_n} + \frac{e_{n;N}^T}{M_n} X \beta_{\bullet, c_n}^0 + \frac{e_{n;N}^T}{M_n} V \tilde{W}^{-1} D_{\tilde{W}} \theta_{\bullet, c_n} \right]}{\sum_{k'=1}^K \exp \left[\alpha_{k'} + \frac{e_{n;N}^T}{M_n} X \beta_{\bullet, k'}^0 + \frac{e_{n;N}^T}{M_n} V \tilde{W}^{-1} D_{\tilde{W}} \theta_{\bullet, k'} \right]} \right) \\
& \times \prod_{s=1}^S \prod_{k=1}^K \left\{ \sigma_{\text{topic}, s} \exp \left(-\frac{\theta_{sk}^2 \sigma_{\text{topic}, s}^2}{2\tau_{s; \theta}^2} \right) \right\} \times \prod_{j=1}^J \prod_{k=1}^K \left\{ \sigma_{\text{obs}, j} \exp \left(-\frac{(\beta_{jk}^0)^2 \sigma_{\text{obs}, j}^2}{2\tau_{j; \beta^0}^2} \right) \right\} \\
& \times \prod_{j=1}^J (\lambda^2)^{\frac{K+1}{2}} (\tau_{j; \beta^0}^2)^{\frac{K+1}{2}-1} \exp \left(-\frac{\lambda^2}{2} \tau_{j; \beta^0}^2 \right) \times \prod_{s=1}^S (\lambda^2)^{\frac{K+1}{2}} (\tau_{s; \theta}^2)^{\frac{K+1}{2}-1} \exp \left(-\frac{\lambda^2}{2} \tau_{s; \theta}^2 \right) \\
& \times (\lambda^2)^{a\lambda-1} e^{-b\lambda\lambda^2} \\
& \times \prod_{n=1}^N \prod_{s=1}^S \prod_{p=1}^P \left(e^{-\tilde{H}_{ns} \tilde{W}_{sp}} (\tilde{H}_{ns} \tilde{W}_{sp})^{Z_{nsp}} \right) \\
& \times \prod_{n=1}^N \prod_{s=1}^S \left(\tilde{H}_{ns}^{a_H-1} e^{-b_H \tilde{H}_{ns}} \right) \times \prod_{s=1}^S \prod_{p=1}^P \left(\tilde{W}_{sp}^{a_W-1} e^{-b_W \tilde{W}_{sp}} \right).
\end{aligned}$$

Now, consider the transformation: $\tilde{\theta}_{sk} = \sigma_{\text{topic}, s} \theta_{sk}$ and $\tilde{\beta}_{jk}^0 = \sigma_{\text{obs}, j} \beta_{jk}^0$. The Jacobians of these transformations are $1/\sigma_{\text{topic}, s}$ and $1/\sigma_{\text{obs}, j}$ respectively. In the matrix form, the transformations can be written as $\tilde{\theta}_{\bullet, k} = D_{\sigma_{\text{topic}}} \theta_{\bullet, k}$ and $\tilde{\beta}_{\bullet, k} = D_{\sigma_{\text{obs}}} \beta_{\bullet, k}$ where $D_{\sigma_{\text{topic}}} = \text{Diag}(\sigma_{\text{topic}, 1}, \dots, \sigma_{\text{topic}, S})$ and $D_{\sigma_{\text{obs}}} = \text{Diag}(\sigma_{\text{obs}, 1}, \dots, \sigma_{\text{obs}, J})$. We shall again consider (MCMC) sampling for these transformed parameters $\tilde{\beta}^0$ and $\tilde{\theta}$; the original parameters β^0 and θ are computed posthoc via transformation. The joint posterior density for $\alpha, \tilde{\beta}^0, \tilde{\theta}, \lambda^2, \{\tau_l^2\}, \{\tilde{H}_{ns}\}$, and $\{\tilde{W}_{sp}\}$ is:

$$\begin{aligned}
& \pi(\alpha, \tilde{\beta}^0, \tilde{\theta}, \lambda^2, \{\tau_l^2\}, \{\tilde{H}_{ns}\}, \{\tilde{W}_{sp}\}, | X, XU, c) \\
& \propto \prod_{n=1}^N \left(\frac{\exp \left[\alpha_{c_n} + \frac{e_{n;N}^T}{M_n} X D_{\sigma_{\text{obs}}}^{-1} \tilde{\beta}_{\bullet, c_n}^0 + \frac{e_{n;N}^T}{M_n} V \tilde{W}^{-1} D_{\tilde{W}} D_{\sigma_{\text{topic}}}^{-1} \tilde{\theta}_{\bullet, c_n} \right]}{\sum_{k'=1}^K \exp \left[\alpha_{k'} + \frac{e_{n;N}^T}{M_n} X D_{\sigma_{\text{obs}}}^{-1} \tilde{\beta}_{\bullet, k'}^0 + \frac{e_{n;N}^T}{M_n} V \tilde{W}^{-1} D_{\tilde{W}} D_{\sigma_{\text{topic}}}^{-1} \tilde{\theta}_{\bullet, k'} \right]} \right) \\
& \times \prod_{s=1}^S \prod_{k=1}^K \left\{ \exp \left(-\frac{\tilde{\theta}_{sk}^2}{2\tau_{s; \theta}^2} \right) \right\} \times \prod_{j=1}^J \prod_{k=1}^K \left\{ \exp \left(-\frac{(\tilde{\beta}_{jk}^0)^2}{2\tau_{j; \beta^0}^2} \right) \right\} \\
& \times \prod_{j=1}^J (\lambda^2)^{\frac{K+1}{2}} (\tau_{j; \beta^0}^2)^{\frac{K+1}{2}-1} \exp \left(-\frac{\lambda^2}{2} \tau_{j; \beta^0}^2 \right) \times \prod_{s=1}^S (\lambda^2)^{\frac{K+1}{2}} (\tau_{s; \theta}^2)^{\frac{K+1}{2}-1} \exp \left(-\frac{\lambda^2}{2} \tau_{s; \theta}^2 \right) \\
& \times (\lambda^2)^{a\lambda-1} e^{-b\lambda\lambda^2}
\end{aligned}$$

$$\begin{aligned}
& \times \prod_{n=1}^N \prod_{s=1}^S \prod_{p=1}^P \left(e^{-\tilde{H}_{ns}\tilde{W}_{sp}} \left(\tilde{H}_{ns}\tilde{W}_{sp} \right)^{Z_{nsp}} \right) \\
& \times \prod_{n=1}^N \prod_{s=1}^S \left(\tilde{H}_{ns}^{a_H-1} e^{-b_H\tilde{H}_{ns}} \right) \times \prod_{s=1}^S \prod_{p=1}^P \left(\tilde{W}_{sp}^{a_W-1} e^{-b_W\tilde{W}_{sp}} \right).
\end{aligned}$$

Below we develop an approximate collapsed Metropolis-within-Gibbs sampler for MCMC sampling from the above posterior. The sampler iteratively draws random elements (MCMC samples) from (a) the conditional posterior $\pi(\tilde{H}, \tilde{W} \mid \alpha, \tilde{\beta}^0, \tilde{\theta}, X, V, c)$ for the *non-normalized* topic model parameters \tilde{H}, \tilde{W} given the multinomial logistic regression (supervised) parameters, and (b) from the conditional posterior $\pi(\alpha, \tilde{\beta}^0, \tilde{\theta}, \lambda^2, \{\tau_l^2\} \mid \tilde{H}, \tilde{W}, X, V, c)$ of the multinomial logistic regression given the topic model parameter induced predictor matrices.

C.1 Approximate sampling from the supervised conditional topic model posterior $\pi(\tilde{H}, \tilde{W} \mid \alpha, \tilde{\beta}^0, \tilde{\theta}, \lambda^2, \{\tau_l^2\}, X, V, c)$

Exploiting the additive property of the Poisson distribution and the multinomial-Poisson connection, we devise a MCMC sampling strategy from the conditional posterior of the supervised conditional topic model. Subsequently, approximate samples from the posterior $\pi(\tilde{H}, \tilde{W}, Z \mid \alpha, \tilde{\beta}^0, \tilde{\theta}, \lambda^2, \{\tau_l^2\}, X, V, c)$ is generated iteratively by first drawing random latent data Z from the conditional density $\pi(Z \mid \tilde{H}, \tilde{W}, \alpha, \tilde{\beta}^0, \tilde{\theta}, X, V, c) = \pi(Z \mid \tilde{H}, \tilde{W}, V)$, and then drawing Markov chain draws for (\tilde{H}, \tilde{W}) from the conditional density $\pi(\tilde{H}, \tilde{W} \mid Z, \alpha, \tilde{\beta}^0, \tilde{\theta}, X, V, c)$.

C.1.1 Drawing $\{Z_{nsp}\}$

Conditional on $V_{np} = \sum_{s=1}^S Z_{nsp}$, the vector $(Z_{n1p}, \dots, Z_{nSp})$ has a multinomial distribution:

$$(Z_{n1p}, \dots, Z_{nSp}) \mid \tilde{H}, \tilde{W}, V \sim \text{Multinomial}(V_{np}, (\phi_{n1p}, \dots, \phi_{nSp}))$$

where $\phi_{nsp} \propto \tilde{H}_{ns}\tilde{W}_{sp}$ and $\sum_{s=1}^S \phi_{nsp} = 1$, and the collection $\{Z_{nsp}\}$ is independent of $\{Z_{n's'p'}\}$ whenever $n \neq n'$ or $p \neq p'$.

C.1.2 Drawing \tilde{H}, \tilde{W} (approximately)

The full conditional density of $\{\tilde{H}_{ns}\}, \{\tilde{W}_{sp}\}$ given the latent data $\{Z_{nsp}\}$, all other parameters and the observed data is given by:

$$\begin{aligned}
& \pi(\{\tilde{H}_{ns}\}, \{\tilde{W}_{sp}\}, \{Z_{nsp}\}, \alpha, \tilde{\beta}^0, \tilde{\theta}, \lambda^2, \{\tau_l^2\}, X, V, c) \\
& \propto \prod_{n=1}^N \prod_{s=1}^S \left(\tilde{H}_{ns}^{a_H-1} e^{-b_H \tilde{H}_{ns}} \right) \times \prod_{s=1}^S \prod_{p=1}^P \left(\tilde{W}_{sp}^{a_W-1} e^{-b_W \tilde{W}_{sp}} \right) \\
& \quad \times \prod_{n=1}^N \prod_{s=1}^S \prod_{p=1}^P \left(e^{-\tilde{H}_{ns} \tilde{W}_{sp}} \left(\tilde{H}_{ns} \tilde{W}_{sp} \right)^{Z_{nsp}} \right) \\
& \quad \times \prod_{n=1}^N \left(\frac{\exp \left[\alpha_{c_n} + \frac{e_{n:N}^T X D_{\sigma_{\text{obs}}}^{-1} \beta_{\bullet, c_n}^0 + \frac{e_{n:N}^T}{M_n} \sum_{s=1}^S (V \tilde{W}^- D_{\tilde{W}})_{\bullet, s} \frac{\tilde{\theta}_{s, c_n}}{\sigma_{\text{topic}, s}} \right]}{\sum_{k'=1}^K \exp \left[\alpha_{k'} + \frac{e_{n:N}^T X D_{\sigma_{\text{obs}}}^{-1} \beta_{\bullet, k'}^0 + \frac{e_{n:N}^T}{M_n} \sum_{s=1}^S (V \tilde{W}^- D_{\tilde{W}})_{\bullet, s} \frac{\tilde{\theta}_{s, k'}}{\sigma_{\text{topic}, s}} \right]} \right) \right).
\end{aligned}$$

To generate approximate samples from the above density a further Gibbs type algorithm will be devised to draw \tilde{H} and \tilde{W} from their corresponding conditional densities.

We first discuss an *exact* Metropolis-within-Gibbs sampler to draw from the above conditional density, and note the computational challenges associated with this sampler. In this sampler, one iteratively draws $\{\tilde{H}_{ns}\}$ from the conditional posterior density given $\{Z_{nsp}\}$, \tilde{W} and the multinomial logistic parameters, and then draws $\{\tilde{W}_{sp}\}$ from its conditional density given \tilde{H} , $\{Z_{nsp}\}$ and the multinomial logistic parameters. The conditional density of $\{\tilde{H}_{ns}\}$ is product gamma which can be effortlessly simulated. The (joint) conditional density of $\{\tilde{W}_{sp}\}$ however is not in a standard form, and has the shape of a product gamma density (contribution from the unsupervised part) multiplied with the product of multinomial logistic likelihood terms (supervised part). In theory one may consider a Metropolis-Hastings MCMC sampling scheme here, by first drawing $\{\tilde{W}_{sp}\}$ proposals from the product Gamma density arising from the unsupervised part, and then performing a Metropolis accept-reject step to account for the contribution of supervised part. A key computational challenge with this approach lies in the evaluation of the generalized inverse matrix \tilde{W}^- which must be evaluated for each proposal of the \tilde{W} matrix which adds substantial computational burden to the entire process. Furthermore, the contribution to the supervised multinomial logistic likelihood of individual data points $\{n\}$ cannot be separated as they all include contributions of the entire \tilde{W} matrix. The collective (product) logistic contributions of all data points however may substantially lower the Metropolis acceptance rate.

Instead, we develop and use the following following *approximate* Metropolis-within-Gibbs sampler for sampling from \tilde{H}, \tilde{W} , by invoking the following approximations.

Approximation 1:

First, we approximate Z_{nsp} in the multinomial logistic term in the above joint density by its conditional expectation $Z_{nsp} \approx E(Z_{nsp} \mid \tilde{H}_{ns}, \tilde{W}_{nsp}) = \tilde{H}_{nsp} \tilde{W}_{sp}$. This is the usual

NMF approximation, and can be viewed as a first order Taylor approximation. Note that this implies $V_{np} = \sum_{s=1}^S Z_{nsp} \approx E(\sum_{s=1}^S Z_{nsp} | \tilde{H}_{ns}, \tilde{W}_{nsp}) = \sum_{s=1}^S \tilde{H}_{ns} \tilde{W}_{sp} = (\tilde{H}\tilde{W})_{sp}$, i.e., $V = XU \approx \tilde{H}\tilde{W}$. Then for each $k = 1, \dots, K$,

$$\begin{aligned} \frac{e_{n;N}^T}{M_n} \sum_{s=1}^S (V\tilde{W}^{-1}D_{\tilde{W}})_{\bullet,s} \frac{\tilde{\theta}_{s,k}}{\sigma_{\text{topic},s}} &\approx \frac{e_{n;N}^T}{M_n} \sum_{s=1}^S (\tilde{H}\tilde{W}\tilde{W}^{-1}D_{\tilde{W}})_{\bullet,s} \frac{\tilde{\theta}_{s,k}}{\sigma_{\text{topic},s}} \\ &= \frac{e_{n;N}^T}{M_n} \sum_{s=1}^S (\tilde{H}D_{\tilde{W}})_{\bullet,s} \frac{\tilde{\theta}_{s,k}}{\sigma_{\text{topic},s}} \\ &= \frac{e_{n;N}^T}{M_n} \sum_{s=1}^S [\tilde{H}]_{\bullet,s} [D_{\tilde{W}}]_{s,s} \frac{\tilde{\theta}_{s,k}}{\sigma_{\text{topic},s}} \\ &= \frac{1}{M_n} \tilde{H}_{ns} [D_{\tilde{W}}]_{s,s} \frac{\tilde{\theta}_{s,k}}{\sigma_{\text{topic},s}} \end{aligned}$$

and

$$\begin{aligned} \sigma_{\text{topic},s} &= g\left([\tilde{X}U\tilde{W}^{-1}D_{\tilde{W}}]_{\bullet,s}\right) \\ &= g\left([D_M^{-1}XU\tilde{W}^{-1}D_{\tilde{W}}]_{\bullet,s}\right) \\ &\approx g\left([D_M^{-1}\tilde{H}D_{\tilde{W}}]_{\bullet,s}\right) \\ &= [D_{\tilde{W}}]_{s,s} g\left(D_M^{-1}[\tilde{H}]_{\bullet,s}\right) \end{aligned}$$

where $[D_{\tilde{W}}]_{s,s} = \sum_{p=1}^P W_{sp}$ is the s -th diagonal entry of $D_{\tilde{W}}$, $[\tilde{H}]_{\bullet,s}$ is the s -th column of \tilde{H} , $D_M = \text{Diag}(M_1, \dots, M_n)$, and g is the sample standard deviation function defined for a vector $t = (t_1, \dots, t_N)$ as $g(t) = \sqrt{\frac{1}{N-1} \sum_{n=1}^N (t_n - \bar{t})^2}$ with $\bar{t} = \frac{1}{N} \sum_{n=1}^N t_n$. Combining, we get

$$\frac{e_{n;N}^T}{M_n} \sum_{s=1}^S (V\tilde{W}^{-1}D_{\tilde{W}})_{\bullet,s} \frac{\tilde{\theta}_{s,k}}{\sigma_{\text{topic},s}} \approx \sum_{s=1}^S \tilde{H}_{ns} \frac{\tilde{\theta}_{s,k}}{M_n g\left(D_M^{-1}[\tilde{H}]_{\bullet,s}\right)}$$

which implies

$$\begin{aligned} &\pi(\{\tilde{H}_{ns}\}, \{\tilde{W}_{sp}\} | \alpha, \tilde{\beta}^0, \tilde{\theta}, \lambda^2, \{\tau_l^2\}, X, V, c) \\ &\propto \prod_{n=1}^N \prod_{s=1}^S (\tilde{H}_{ns}^{\alpha_H - 1} e^{-b_H \tilde{H}_{ns}}) \times \prod_{s=1}^S \prod_{p=1}^P (\tilde{W}_{sp}^{\alpha_W - 1} e^{-b_W \tilde{W}_{sp}}) \\ &\quad \times \prod_{n=1}^N \prod_{s=1}^S \prod_{p=1}^P \left(e^{-\tilde{H}_{ns} \tilde{W}_{sp}} (\tilde{H}_{ns} \tilde{W}_{sp})^{Z_{nsp}} \right) \end{aligned}$$

$$\times \prod_{n=1}^N \left(\frac{\exp \left[\alpha_{c_n} + \frac{e_{n;N}^T X D_{\sigma_{\text{obs}}}^{-1} \tilde{\beta}_{\bullet, c_n}^0 + \sum_{s=1}^S \tilde{H}_{ns} \frac{\tilde{\theta}_{s, c_n}}{M_n g(D_M^{-1}[\tilde{H}]_{\bullet, s})} \right]}{\sum_{k'=1}^K \exp \left[\alpha_{k'} + \frac{e_{n;N}^T X D_{\sigma_{\text{obs}}}^{-1} \tilde{\beta}_{\bullet, k'}^0 + \sum_{s=1}^S \tilde{H}_{ns} \frac{\tilde{\theta}_{s, k'}}{M_n g(D_M^{-1}[\tilde{H}]_{\bullet, s})} \right]} \right)$$

There are two major consequences of this approximation. First, the approximate joint conditional posterior density does not involve the generalized inverse matrix \tilde{W}^{-} any more, which effectuates significant reduction in the overall computation burden. Second, the full conditional (given $\{\tilde{H}_{ns}\}$ and other parameters) joint posterior density of $\{\tilde{W}_{sp}\}$ reduces to a product univariate gamma form:

$$\pi(\{\tilde{W}_{sp}\} \mid \{\tilde{H}_{ns}\}, \alpha, \beta^0, \theta, \lambda^2, \{\tau_l^2\}, X, V, c) \propto \prod_{s=1}^S \prod_{p=1}^P \left(\tilde{W}_{sp}^{a_W + \sum_{n=1}^N Z_{nsp} - 1} e^{-(b_W + \sum_{n=1}^N \tilde{H}_{ns}) \tilde{W}_{sp}} \right).$$

This implies that conditional on the other parameters, the entries of the \tilde{W} matrix can be effortlessly and independently sampled from univariate gamma distributions, which leads to the following step for the MCMC sampling.

1. **Drawing \tilde{W} .** Generate $\{\tilde{W}_{sp}\}$ independently from the following full conditional Gamma distribution:

$$\tilde{W}_{sp} \mid Z, \tilde{H}, \alpha, \beta^0, \theta, \lambda^2, \{\tau_l^2\}, X, V, c \stackrel{a}{\sim} \text{Gamma} \left(a_W + \sum_{n=1}^N Z_{nsp}, b_W + \sum_{n=1}^N \tilde{H}_{ns} \right).$$

However, the approximate full conditional joint density of $\{\tilde{H}_{ns}\}$ given $\{\tilde{W}_{sp}\}$ and other parameters still has an intractable form due to the softmax (multinomial) probabilities which also include the computed sample standard deviation terms. Note that, for each topic s , the approximate sample standard deviation term $g(D_M^{-1}[\tilde{H}]_{\bullet, s})$ involves all rows of the matrix column $\tilde{H}_{\bullet, s}$ arising out of different $\{n\}$, and the multinomial logistic contribution of each observation n involves all topics s . In other words, the elements of \tilde{H} cannot be independently sampled, even when conditioned on \tilde{W} and Z . We propose the following *independent* Metropolis-Hastings sampler that generates each row of \tilde{H} sequentially conditional on all other rows of \tilde{H} . An approximation that reduces the computational load and encourages better mixing by removing the dependence across rows is discussed afterward.

2. **Drawing the rows of \tilde{H} .** Let \tilde{H}^{old} denote the current state of \tilde{H} . Each row of \tilde{H} is drawn sequentially conditional on the other rows. To update the n -th row first draw a proposal vector $\tilde{H}_{n, \bullet}^{\text{prop}} = (\tilde{H}_{n1}^{\text{prop}}, \dots, \tilde{H}_{nS}^{\text{prop}})$ utilizing the independent unsupervised

Poisson contribution for the each augmented count $\{Z_{nsp}\}$:

$$\tilde{H}_{ns}^{\text{prop}} \mid Z, \tilde{W}, X, V \stackrel{a}{\sim} \text{Gamma} \left(a_H + \sum_{p=1}^P Z_{nsp}, b_H + \sum_{p=1}^P \tilde{W}_{sp} \right).$$

With these proposal values $\{\tilde{H}_{ns}^{\text{prop}}\}$ for the n -th row and keeping the other rows fixed at their current states, compute (update) the sample standard deviation terms $\tilde{\sigma}_s = \tilde{\sigma}_s([\tilde{H}]_{\bullet,s}) = g \left(D_M^{-1} [\tilde{H}]_{\bullet,s} \right)$. Call the corresponding (proposal) value of $\tilde{\sigma}_s$ as $\tilde{\sigma}_s^{\text{prop}}$ and the current value of $\tilde{\sigma}_s$ as σ_s^{prop} . Next compute the acceptance ratio

$$r \left(\tilde{H}_{n,\bullet}^{\text{prop}} \mid \tilde{H}_{n,\bullet}^{\text{old}} \right) = \left(\frac{\exp \left[\alpha_{c_n} + \frac{e_{n:N}^T X D_{\sigma_{\text{obs}}}^{-1} \tilde{\beta}_{\bullet,c_n}^0 + \sum_{s=1}^S \tilde{H}_{ns}^{\text{prop}} \frac{\tilde{\theta}_{s,c_n}}{M_n \tilde{\sigma}_s^{\text{prop}}} \right]}{\sum_{k'=1}^K \exp \left[\alpha_{k'} + \frac{e_{n:N}^T X D_{\sigma_{\text{obs}}}^{-1} \tilde{\beta}_{\bullet,k'}^0 + \sum_{s=1}^S \tilde{H}_{ns}^{\text{prop}} \frac{\tilde{\theta}_{s,k'}}{M_n \sigma_s^{\text{prop}}} \right]} \right) \times \left(\frac{\exp \left[\alpha_{c_n} + \frac{e_{n:N}^T X D_{\sigma_{\text{obs}}}^{-1} \tilde{\beta}_{\bullet,c_n}^0 + \sum_{s=1}^S \tilde{H}_{ns}^{\text{old}} \frac{\tilde{\theta}_{s,c_n}}{M_n \sigma_s^{\text{old}}} \right]}{\sum_{k'=1}^K \exp \left[\alpha_{k'} + \frac{e_{n:N}^T X D_{\sigma_{\text{obs}}}^{-1} \tilde{\beta}_{\bullet,k'}^0 + \sum_{s=1}^S \tilde{H}_{ns}^{\text{old}} \frac{\tilde{\theta}_{s,k'}}{M_n \sigma_s^{\text{old}}} \right]} \right)^{-1}$$

and draw $U \sim \text{Uniform}(0, 1)$. Then update the n -th row of \tilde{H} by $\tilde{H}_{n,\bullet}^{\text{prop}}$ if $U < r(\tilde{H}_{n,\bullet}^{\text{prop}} \mid \tilde{H}_{n,\bullet}^{\text{old}})$ or leave the row unchanged otherwise. We note that this one-step Metropolis adjustment for the entire n -th row for \tilde{H} may have low acceptance rate if the choices of the regression coefficient $\{\theta_{sp}\}$ are poor, and/or the total number of topics S is large. For large S (say $S \geq 50$) we recommend partitioning each row into multiple smaller dimensional random blocks and then performing the above independent Metropolis-Hastings sampling separately on each block conditioning the remaining blocks. Simultaneously, the Metropolis accept-reject step for each row proposal may be performed multiple times with independent, new proposals, until a reasonable (say 90%¹) overall acceptance rate is achieved.

Approximation 2:

The serial dependence among the rows of \tilde{H} and the overall computational burden can be reduced by assuming $\tilde{\sigma}_s([\tilde{H}]_{\bullet,s}) = g \left(D_M^{-1} [\tilde{H}]_{\bullet,s} \right)$ to be approximately fixed across iterations, say at $\tilde{\sigma}_s^{\text{fixed}}$. This can be a reasonable approximation when the sample size N is large and the Markov chain is stationary; in which case the $\tilde{\sigma}_s([\tilde{H}]_{\bullet,s}) \approx \sigma_s^{\text{popn}}$. Here σ_s^{popn} denotes the population (associated with the tumor samples $\{n\}$) level standard deviation of the exposure from the s -th topic (cataloged along the rows of $D_M^{-1} [\tilde{H}]_{\bullet,s}$). Then, the Metropolis

¹Note that the proposed Metropolis sampler is an independence sampler, and not a random-walk Metropolis algorithm. Unlike random-walk Metropolis algorithms, independence Metropolis samplers do not require manual tuning, and can achieve better convergence than random walk samplers depending on the problem.

acceptance ratio becomes

$$\tilde{r} \left(\tilde{H}_{n,\bullet}^{\text{prop}} \mid \tilde{H}_{n,\bullet}^{\text{old}} \right) = \left(\frac{\exp \left[\alpha_{c_n} + \frac{e_{n;N}^T}{M_n} X D_{\sigma_{\text{obs}}}^{-1} \tilde{\beta}_{\bullet,c_n}^0 + \sum_{s=1}^S \tilde{H}_{ns}^{\text{prop}} \frac{\tilde{\theta}_{s,c_n}}{M_n \tilde{\sigma}_s^{\text{fixed}}} \right]}{\sum_{k'=1}^K \exp \left[\alpha_{k'} + \frac{e_{n;N}^T}{M_n} X D_{\sigma_{\text{obs}}}^{-1} \tilde{\beta}_{\bullet,k'}^0 + \sum_{s=1}^S \tilde{H}_{ns}^{\text{prop}} \frac{\tilde{\theta}_{s,k'}}{M_n \tilde{\sigma}_s^{\text{fixed}}} \right]} \right) \times \left(\frac{\exp \left[\alpha_{c_n} + \frac{e_{n;N}^T}{M_n} X D_{\sigma_{\text{obs}}}^{-1} \tilde{\beta}_{\bullet,c_n}^0 + \sum_{s=1}^S \tilde{H}_{ns}^{\text{old}} \frac{\tilde{\theta}_{s,c_n}}{M_n \tilde{\sigma}_s^{\text{fixed}}} \right]}{\sum_{k'=1}^K \exp \left[\alpha_{k'} + \frac{e_{n;N}^T}{M_n} X D_{\sigma_{\text{obs}}}^{-1} \tilde{\beta}_{\bullet,k'}^0 + \sum_{s=1}^S \tilde{H}_{ns}^{\text{old}} \frac{\tilde{\theta}_{s,k'}}{M_n \tilde{\sigma}_s^{\text{fixed}}} \right]} \right)^{-1}$$

Consequently, under this approximation, the Metropolis steps for each row of \tilde{H} can be performed independently, permitting better mixing, and reduction in the computation load (due to iterative updating of the standard deviation terms), at the cost of some (possibly small) approximation error.

C.2 Sampling from the conditional multinomial logistic model posterior given topic model parameters

We develop the following data augmentation Gibbs sampler for MCMC sampling from the conditional, group-lasso regularized, multinomial logistic posterior given the topic model parameters. Conditional on the topic model, the multinomial logistic regression entails predicting the cancer site probabilities $\{\text{Pr}(c = k)\}$ given the topic model induced *row-normalized* and *column standard-deviation scaled* stacked design matrix $(1, D_M^{-1} X D_{\sigma_{\text{obs}}}^{-1}, D_M^{-1} X U W^{-1} D_{\sigma_{\text{topic}}}^{-1})$. Let $L = (S + J)$, and construct the collected regression coefficient matrix δ by stacking the rows of β^0 and θ matrices; the k -th column of δ is thus given by

$$\delta_{\bullet,k} = \begin{pmatrix} \tilde{\beta}_{1,k}^0 \\ \vdots \\ \tilde{\beta}_{J,k}^0 \\ \tilde{\theta}_{1,k} \\ \vdots \\ \tilde{\theta}_{S,k} \end{pmatrix}.$$

We index the rows of δ by $l; l = 1, \dots, L$. The proposed Gibbs sampler utilizes the Pólya-Gamma data augmentation scheme for (multinomial) logistic regression model (Polson, Scott, and Windle 2013) and the Gibbs sampler for hierarchical group-lasso regularized linear regression (Casella et al. 2010). At each iteration, the sampler iterates between drawing the sparsity handling variance parameters $\{\tau_l^2\}$ and λ^2 , and the multinomial logistic parameters

α , and δ .

C.2.1 Drawing the sparsity handling parameters

1. **Drawing** $\{\tau_l^2\}$. Draw the reciprocals $\{1/\tau_l^2 : l = 1, \dots, L\}$ independently from the following conditional posterior distributions:

$$1/\tau_l^2 \mid \{\delta\}, \lambda \sim \begin{cases} \text{inverse-Gamma} \left(\frac{1}{2}, \frac{\lambda^2}{2} \right) & \|\delta_{l,\bullet}\| = 0 \\ \text{inverse-Gaussian} \left(\sqrt{\frac{\lambda^2}{\|\delta_{l,\bullet}\|^2}}, \lambda^2 \right) & \|\delta_{l,\bullet}\| > 0 \end{cases}$$

and subsequently compute $\{\tau_l^2 : l = 1, \dots, D\}$.

2. **Drawing** λ^2 : Generate λ^2 from its conditional posterior density given τ_l^2 :

$$\lambda^2 \mid \{\tau_l^2\} \sim \text{Gamma} \left(a_\lambda + \frac{K(L+1)}{2}, b_\lambda + \frac{\sum_{l=1}^L \tau_l^2}{2} \right).$$

C.2.2 Drawing augmented data and multinomial logistic regression parameters

First define the derived conditional design matrix \tilde{X} by column stacking:

$$\tilde{X} = \left(1 : D_M^{-1} X D_{\sigma_{\text{obs}}}^{-1} : D_M^{-1} X U W^{-1} D_{\sigma_{\text{topic}}}^{-1} \right)$$

and denote the rows of \tilde{X} as \tilde{x}_n ; $n = 1, \dots, N$. Next separately for each cancer site $k = 1, \dots, K$ iteratively update the associated intercept and regression coefficients $\tilde{\delta}_k = (\alpha_k, \delta_{\bullet,k}^T)^T$ conditional on those for the other cancer sites $k' \neq k$ utilizing a Pólya-Gamma data augmentation scheme (Polson, Scott, and Windle 2013) as follows.

1. **Generate Pólya-Gamma augmented data** $\{\gamma_{nk}\}$. Calculate

$$g_{nk} = \log \left(\sum_{k' \neq k} \tilde{x}_n^T \tilde{\delta}_{k'} \right); G_{nk} = \tilde{x}_n^T \tilde{\delta}_k - g_{nk}$$

and draw the augmented data $\{\gamma_{nk} : n = 1, \dots, k\}$ from the Pólya-Gamma distribution (Polson, Scott, and Windle 2013)

$$\gamma_{nk} \mid \text{rest} \sim \text{PG}(1, g_{nk}).$$

and define $\Gamma_k = \text{Diag}(\gamma_{1k}, \dots, \gamma_{nk})$.

2. **Generate multinomial logistic intercept and regression parameters.** Calculate

B_k and μ_k as follows

$$B_k^{-1} = \begin{pmatrix} \tilde{X}^T & \Gamma_k & \tilde{X} \end{pmatrix} + \text{Diag}(1/\sigma_{\alpha,0k}^2, 1/\tau_1^2, \dots, 1/\tau_L^2)$$

and

$$\mu_k = B_k \tilde{X}^T \left(\left[y_{\bullet,k} - \frac{1}{2} \right] + \Gamma_k C_{\bullet,k} \right)$$

where $y_{\bullet,k}$ is the k -th column of the binary cancer site indicator matrix $((y_{nk}))$ with $y_{nk} = I(c_n = k)$ and $C_{\bullet,k}$ is the k -th column of the matrix $((C_{nk}))$. The intercept α_k and the regression coefficients $\delta_{\bullet,k}$ are then jointly generated from the conditional multivariate normal distribution:

$$\tilde{\delta}_k = (\alpha_k, \delta_{\bullet,k}^T)^T \mid \text{rest} \sim N_{1+L}(\mu_k, B_k)$$

D Initialization of the MCMC algorithm

The MCMC algorithm is initialized at the approximate marginal posterior mode of the model. To this end, we first obtain the marginal posterior mode of the multi-logistic intercept α , regression coefficients for the residual variant effects β^0 and the *observed* meta-feature effects ω using the group-lasso based point estimation method of (Chakraborty, Begg, and Shen 2020) on the training data using the row normalized versions of the mutation counts X and XU . The associated cross-validation based optimal value of the group lasso penalty parameter λ is also noted. Next, we perform frequentist unsupervised NMF estimation (DeBruine 2021) on the columns of XU to obtain initial estimates of H and W . The initial values of the regression coefficients θ for the *latent topics* are then obtained as $\theta = W\omega$. These initial values of the parameter α , β^0 , θ , H and W are then used as then used to generate initial values of the remaining parameters $\{\tau_l^2\}$ based on the MCMC sampling scheme.

E Association of the “Liver” window topic-specific composition probabilities (Figure 2A in the main text) with H3K4me1 Histone Marks

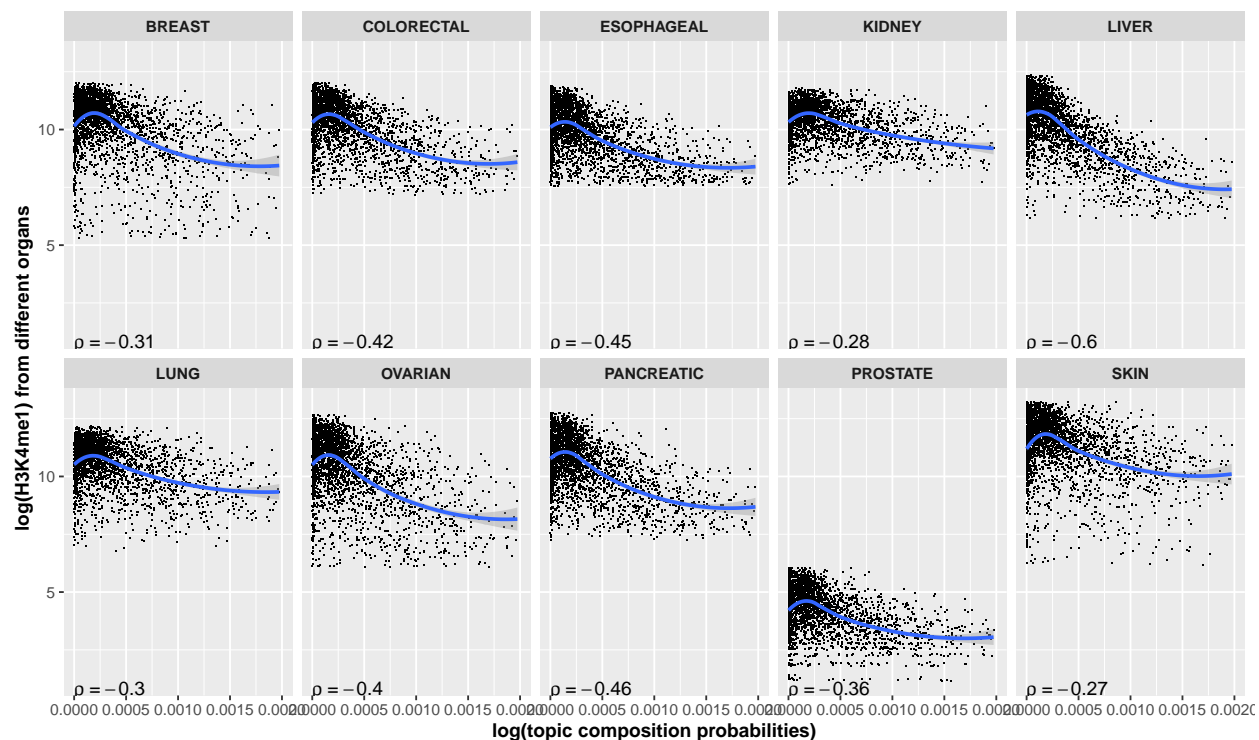


Figure S1: Points in the scatters display the log composition probabilities for the "liver" topic (displayed on Figure 2A in the main text) along the x-axes and log epigenomic features (histone marks H3k4me1) along the y-axes for all ~ 3000 chromosome window meta-feature categories. Different site-specific epigenome scores are plotted along different panels. Inscribed at the bottom-left corner of each panel is the Spearman correlation coefficient ρ between the corresponding topic composition probabilities and H3k4me1 scores.

References

- Blei, David M., Andrew Y. Ng, and Michael I. Jordan. 2003. "Latent Dirichlet Allocation." *Journal of Machine Learning Research* 3 (Jan): 993–1022. <https://www.jmlr.org/papers/v3/blei03a>.
- Casella, George, Malay Ghosh, Jeff Gill, and Minjung Kyung. 2010. "Penalized Regression, Standard Errors, and Bayesian Lassos." *Bayesian Analysis* 5 (2): 369–411.
- Chakraborty, Saptarshi, Colin B. Begg, and Ronglai Shen. 2020. "Using the "Hidden" genome to improve classification of cancer types." *Biometrics*, September.
- DeBruine, Zachary. 2021. *RcppML: Rcpp Machine Learning Library*.
- Polson, Nicholas G., James G. Scott, and Jesse Windle. 2013. "Bayesian Inference for Logistic Models Using Pólya–Gamma Latent Variables." *J Am Stat Assoc* 108 (504): 1339–49. <https://doi.org/10.1080/01621459.2013.829001>.